Large protein complexes retained in the ER are dislocated by non-COPII vesicles and degraded by selective autophagy

Le Fourn, Valerie ; Park, Sujin ; Jang, Insook ; Gaplovska-Kysela, Katarina ; Guhl, Bruno ; Lee, Yangsin ; Cho, Jin Won ; Zuber, Christian ; Roth, Jürgen

Abstract: Multisubunit protein complexes are assembled in the endoplasmic reticulum (ER). Existing pools of single subunits and assembly intermediates ensure the efficient and rapid formation of complete complexes. While being kinetically beneficial, surplus components must be eliminated to prevent potentially harmful accumulation in the ER. Surplus single chains are cleared by the ubiquitin-proteasome system. However, the fate of not secreted assembly intermediates of multisubunit proteins remains elusive. Here we show by high-resolution double-label confocal immunofluorescence and immunogold electron microscopy that naturally occurring surplus fibrinogen A - assembly intermediates in HepG2 cells are dislocated together with EDEM1 from the ER to the cytoplasm in ER-derived vesicles not corresponding to COPII-coated vesicles originating from the transitional ER. This route corresponds to the novel ER exit path we have previously identified for EDEM1 (Zuber et al. Proc Natl Acad Sci USA 104:4407-4412, 2007). In the cytoplasm, detergent-insoluble aggregates of fibrinogen A - dimers develop that are targeted by the selective autophagy cargo receptors p62/SQSTM1 and NBR1. These aggregates are degraded by selective autophagy as directly demonstrated by high-resolution microscopy as well as biochemical analysis and inhibition of autophagy by siRNA and kinase inhibitors. Our findings demonstrate that different pathways exist in parallel for ER-to-cytoplasm dislocation and subsequent proteolytic degradation of large luminal protein complexes and of surplus luminal single-chain proteins. This implies that ER-associated protein degradation (ERAD) has a broader function in ER proteostasis and is not limited to the elimination of misfolded glycoproteins.

DOI: https://doi.org/10.1007/s00018-012-1236-6

Cell. Mol. Life Sci. (2013) 70:1985–2002
DOI 10.1007/s00018-012-1236-6

Cellular and Molecular Life Sciences

RESEARCH ARTICLE

Large protein complexes retained in the ER are dislocated by non-COPII vesicles and degraded by selective autophagy

Valerie Le Fourn · Sujin Park · Insook Jang · Katarina Gaplovska-Kysela · Bruno Guhl · Yangsin Lee · Jin Won Cho · Christian Zuber · Jürgen Roth

Received: 9 August 2012 / Revised: 16 November 2012 / Accepted: 5 December 2012 / Published online: 22 January 2013

Abstract Multisubunit protein complexes are assembled in the endoplasmic reticulum (ER). Existing pools of single subunits and assembly intermediates ensure the efficient and rapid formation of complete complexes. While being kinetically beneficial, surplus components must be eliminated to prevent potentially harmful accumulation in the ER. Surplus single chains are cleared by the ubiquitin–proteasome system. However, the fate of not secreted assembly intermediates of multisubunit proteins remains elusive. Here we show by high-resolution double-label confocal immunofluorescence and immunogold electron microscopy that naturally occurring surplus fibrinogen Aα–γ assembly intermediates in HepG2 cells are dislocated together with EDEM1 from the ER to the cytoplasm in ER-derived vesicles not corresponding to COPII-coated vesicles originating from the transitional ER. This route corresponds to the novel ER exit path we have previously identified for EDEM1 (Zuber et al. Proc Natl Acad Sci USA 104:4407–4412, 2007). In the cytoplasm, detergent-insoluble aggregates of fibrinogen Aα–γ dimers develop that are targeted by the selective autophagy cargo receptors p62/SQSTM1 and NBR1. These aggregates are degraded by selective autophagy as directly demonstrated by high-resolution microscopy as well as biochemical analysis and inhibition of autophagy by siRNA and kinase inhibitors. Our findings demonstrate that different pathways exist in parallel for ER-to-cytoplasm dislocation and subsequent proteolytic degradation of large luminal protein complexes and of surplus luminal single-chain proteins. This implies that ER-associated protein degradation (ERAD) has a broader function in ER proteostasis and is not limited to the elimination of misfolded glycoproteins.

Keywords Endoplasmic reticulum · Protein assembly · Fibrinogen dimer · Protein dislocation · ERAD · Selective autophagy · EDEM1

V. Le Fourn, S. Park, and I. Jang equally contributed to this study.

Electronic supplementary material The online version of this article (doi:10.1007/s00018-012-1236-6) contains supplementary material, which is available to authorized users.

V. Le Fourn · K. Gaplovska-Kysela · B. Guhl · C. Zuber · J. Roth
Division of Cell and Molecular Pathology, Department of Pathology, University of Zurich, 8091 Zurich, Switzerland

S. Park · Y. Lee · J. W. Cho · J. Roth (✉)
Department of Integrated OMICS for Biomedical Science, WCU Program, Yonsei University Graduate School, 50 Yonsei-ro, Seodaemun-gu, Seoul 120-749, Korea
e-mail: jurgen.roth@yonsei.ac.kr

I. Jang · J. W. Cho
Department of Systems Biology, Yonsei University, Seoul 120-749, Korea

Present Address:
V. Le Fourn
Selexis SA, 1228 Plan-les-Ouates/Geneva, Switzerland

Present Address:
K. Gaplovska-Kysela
Department of Genetics, Comenius University, 84215 Bratislava, Slovak Republic

Introduction

The mechanism through which proteins that are retained in the endoplasmic reticulum (ER) become degraded is a question of fundamental importance for ER proteostasis [2, 3]. Non-stoichiometric synthesis of individual components is often observed for multisubunit membrane and secretory proteins and the resulting surplus components are not exported from the ER to the Golgi apparatus [4–6]. This

phenomenon is exemplified by fibrinogen, a multisubunit secretory protein synthesized by the liver, which plays a crucial role in hemostasis and thrombosis [7]. Hepatocytes from various vertebrate species synthesize unequal amounts of the three fibrinogen chains [8]. In human hepatoma HepG2 cells, Aα and γ chains are synthesized in surplus of Bβ chains. Hence, Bβ chains are rate-limiting for the formation of fibrinogen.

Mature fibrinogen is composed of two disulfide-bonded identical half molecules, each consisting of an Aα, Bβ and γ chain linked at their amino termini by numerous interchain disulfide bonds [8, 9]. The assembly of fibrinogen from the three single chains occurs through the rapid and ordered formation of dimers and trimers. Two types of dimers are formed in the ER: predominantly Aα–γ, and to a lesser extent of Bβ–γ dimers. Both types of dimer give rise to the trimeric Aα–Bβ–γ half molecule [10, 11]. The fibrinogen Aα–γ dimers are linked by interchain disulfide bonds at their N-terminal E domain [7, 12–14]. The fully assembled fibrinogen molecules, after transport to the Golgi apparatus, are constitutively secreted. In contrast, the surplus fibrinogen single γ chains and the Aα–γ dimers are not secreted. To prevent their accumulation in the ER, which could result in ER stress and subsequent cell damage [15], they must be degraded.

Previous work has shown the importance of the ubiquitin–proteasome system for the regulated degradation of surplus single subunits of multisubunit proteins. For instance, the T cell antigen receptor (TCR) CD3-δ and α chain subunits that are retained in the ER become ubiquitinated and degraded by the proteasome [16–20]. In immature thymocytes, the ER-associated degradation of native TCR subunits is of importance for the regulation of cell surface expression of TCRs [21, 22]. Although likely, it is currently not known whether the clearance of TCR single chains involves the core components Hrd1p/Hrd3p and Doa10p identified for the ER-associated degradation (ERAD) of mutant membrane proteins [23, 24]. Similar to TCR single chains, the clearance of ER-retained surplus single fibrinogen γ chains has been shown to occur through ubiquitination and proteasomal degradation [25, 26]. It is unknown whether the Hrd1p complex for the clearance of misfolded luminal proteins by ERAD-L [23, 27, 28] is involved in the dislocation of luminal single fibrinogen chains. However, it is tempting to speculate that analogous mechanisms operate for the ER-to-cytoplasm dislocation of ER-retained single TCR subunits or single fibrinogen chains and of misfolded mutant membrane or secretory proteins.

In contrast to single fibrinogen chains, the clearance mechanism of surplus Aα–γ dimeric assembly intermediates is undefined. Recently, we identified by high-resolution immunoelectron microscopy and serial section immunoelectron microscopy a novel vesicular ER exit pathway taken by the ERAD component EDEM1, which does not involve COPII-coated vesicles formed at the transitional ER [1]. EDEM1 (ER degradation-enhancing α mannosidase-like protein 1) has been shown to be involved in routing of misfolded luminal glycoproteins for ERAD [29–33] by its function as an α1,2 mannosidase [33–36] and its interaction with SEL1p [31]. The EDEM1 vesicular pathway involves the formation of ≥150-nm vesicles that lack a recognizable cytosolic coat [1] and that are larger than the standard 60 to 90-nm COPII-coated vesicles [37]. The EDEM1-containing vesicles originate at simple rough ER cisternae rather than the ER exit sites of the transitional ER. We previously demonstrated this by double-label confocal immunofluorescence for EDEM1 and Sec23 and by serial section immunoelectron microscopy [1]. Therefore, this is a pathway distinct from that for the formation of COPII-coated vesicles, which occurs at the specialized transitional ER [38].

Like the ERAD machinery components glucosidase II [39] and ER mannosidase I [40], EDEM1 has a short half-life of ≤1 h [41, 42]. The vesicular ER exit pathway is of importance for the regulated degradation of EDEM1 [41, 42], which occurs by autophagy [41]. At present, it is not known whether the vesicular ER exit route functions solely as a pathway for the degradation of EDEM1 or if it is of general relevance for a broader array of mechanisms involving the dislocation of proteins from the ER to the cytoplasm. To this end, we reasoned that it could provide an exit route for large protein complexes as represented by ER-retained assembly intermediates of multisubunit proteins.

In the present study, we discovered that naturally occurring surplus fibrinogen Aα–γ assembly intermediates together with EDEM1 are dislocated to the cytoplasm in ER-derived vesicles not corresponding to COPII vesicles from the transitional ER. In the cytoplasm, the vesicle membrane is dissolved by an as yet unknown mechanism and aggregates of fibrinogen Aα–γ dimers with the selective autophagy cargo receptors p62/SQSTM1 (sequestosome 1) and NBR1 (neighbor of BRCA1 gene 1) are formed prior to degradation by selective autophagy. Our work demonstrates that different routes for ER-to-cytoplasm dislocation exist in parallel for large luminal protein complexes such as surplus assembly intermediates of fibrinogen and luminal single-chain proteins such as surplus single fibrinogen chains. Hence, this suggests that ER-associated protein degradation (ERAD) has a broader function that extends beyond the elimination of misfolded glycoproteins.

Materials and methods

Cell culture and reagents

Human HepG2 cells were obtained from ATCC (Manassas, VA) and cultured in complete culture medium (Minimum

essential medium; Eagle, Gibco, Auckland, NZ) supplemented with 10 % fetal bovine serum (Gibco) and 1.0 mM sodium pyruvate (Gibco). Cell cultures were replenished with fresh medium 16 h before biochemical analysis or processing for microscopy.

Pepstatin A (P5318), E64d (E8640), vinblastine (V1377), bovine serum albumin (A3156, BSA), Brefeldin A (B7651), diaminobenzidine tetrahydrochloride (D5905, DAB), 3-methyladenine (M9281), wortmannin (w1628), trichostatin A (T8552-1MG), epoxomicin (E3652), OptiPrep density gradient medium (D1556), sodium deoxycholate (D6750), and saponin (S4521) were from Sigma-Aldrich (St. Louis, MO, USA), MG 312 (474790) and ALLN (208719) from Calbiochem (San Diego, CA, USA), glutaraldehyde and osmium tetroxide from EMD (Gibbstown, NJ, USA), paraformaldehyde from Merck (Basel, Switzerland), protease inhibitor cocktail from Roche Applied Science (Basel, Switzerland), and Epon-Araldite kits from Fluka (Buchs, Switzerland). All other chemicals were of p.a. grade and from Sigma-Aldrich. Magnetic beads linked to protein A were purchased from Dynal (Hamburg, Germany).

Rabbit polyclonal antibodies against human fibrinogen reactive with Aα, Bβ and γ chains were obtained from Dako (A0080, Dako Cytomation, Denmark) and rabbit antibodies against the Aα chain of fibrinogen (H-300), goat anti-human EDEM1 antibody against a C-terminal peptide (C-19) as well as rabbit or goat polyclonal antibodies against LC3 (H50, N20) were from Santa Cruz Biotechnology (Santa Cruz, CA, USA) and MBL International (PM036; Woburn, MA, USA). Affinity-purified rabbit polyclonal anti-peptide antibody against EDEM1 was purchased from Sigma (E8406), mouse monoclonal antibodies against LC3 (152-3) were from MBL International and NBR1 (H00004077) were from Novus Biologicals (Littletown, CO, USA) and guinea pig polyclonal antibodies against a C-terminal peptide of human p62/SQSTM1 (GP62-C) from PROGEN (Heidelberg, Germany). Mouse anti-GAPDH antibody (437000) was obtained from Ambion (Applied Biosystems/Ambion, Austin, TX, USA), rabbit anti-ATG5 antibody (2630S) from Cell Signaling Technology and rabbit anti-GRP78 (BiP, SPA-826) as well as mouse anti-PDI antibody (SPA-891) from Stressgen Bioreagent (Victoria, Canada). Horseradish peroxidase-conjugated Fab_2 goat anti-rabbit IgG antibodies, DyLight488-conjugated affinity-purified $F(ab)_2$ fragments of donkey anti-goat IgG, rhodamine Red-X-conjugated affinity-purified donkey anti-rabbit IgG, Cy2-conjugated affinity-purified donkey anti-guinea pig IgG, Cy2-conjugated affinity-purified $F(ab)_2$ fragments of donkey anti-mouse IgG, and AMCA-conjugated affinity-purified $F(ab)_2$ fragments of donkey anti-guinea pig IgG as well as 12-nm gold-labeled affini-pure donkey anti-rabbit IgG (711-205-152) and donkey anti-goat IgG (703-205-155), and 6-nm gold-labeled affini-pure donkey anti-guinea pig IgG (706-195-148), donkey anti-mouse IgG (715-195-150) and donkey anti-rabbit IgG (711-195-152) were from Jackson ImmunoResearch Laboratories, Inc. (West Grove, PA, USA) and Alexa 488 donkey anti-rabbit IgG from Molecular Probes-Invitrogen (Carlsbad, CA, USA). Protein A-gold complexes were prepared according to standard protocol [43, 44].

Short interfering RNA (siRNA) transfection

Double-stranded siRNA targeting human *ATG5*, *ATG7*, and *ATG12* (purchased from Invitrogen) were administered simultaneously (80 nM each) to HepG2 cells (2×10^5) in Metafectene reagent according to the manufacture's instructions (Biontex Laboratories GmbH, Germany). In all experiments, scrambled siRNA served as a control. Cells were analyzed 48 h post-transfection.

Pulse-chase experiments and immunoprecipitation

HepG2 cells grown to about 40 % confluence in complete culture medium (Minimum essential medium; Eagle, Gibco, Auckland, NZ) supplemented with 10 % fetal bovine serum (Gibco) and 1.0 mM sodium pyruvate (Gibco) were fed with fresh medium 16 h before metabolic labeling. For pulse-chase experiments, cells were rinsed quickly once in methionine and cysteine-free MEM (Sigma), pulsed for 20 min with ^{35}S methionine-cysteine (100 mCi/ml; NEN, Boston, MA, USA) in methionine and cysteine-free MEM, washed four times in complete medium and chased in complete medium supplemented with 4 mM of each methionine and cysteine in the absence or presence of the following drugs: leupeptin (100 μg/ml), pepstatin A and E64d (100 μM each), Brefeldin A (10 μg/ml), MG132 (20 μM), ALLN (100 mM), epoxomicin (1 μM), 3-methyladenine (10 mM), and DMSO as control. At the end of the pulse or the chase, cells were washed twice in cold PBS (10 mM phosphate buffer, pH 7.4, 0.15 M NaCl) and mechanically removed. Cell pellets were solubilized in lysis buffer (PBS supplemented with 1 % Triton X-100 and protease inhibitor cocktail) for 30 min at 4 °C and immunoprecipitated. For immunoprecipitation of fibrinogen, lysates were incubated overnight at 4 °C with protein A-Dynal magnetic beads (Invitrogen, Dynal AS, Oslo, Norway) coated with rabbit anti-human fibrinogen antibodies reactive with Aα, Bβ and γ chains. Afterwards, immunocomplexes were washed four times in PBS containing 0.5 % Triton X-100 and electrophoretically resolved under non-reducing conditions in 4–10 % SDS-PAG or reducing conditions in 7.5 % SDS-PAG and subjected to autoradiography. Bands were quantified using ImageQuant TL software (GE Healthcare, Bio-Science) or ImageJ 1.38r (http://rsb.info.nih.gov/ij).

Protein cross-linking and combined immunoprecipitation-Western blot

HepG2 cells were washed with PBS (pH 8) and incubated with 0.5 mM or 1 mM DSP (dithiobis[succinimidyl] propionate, 22586; Pierce, Rockford, IL, USA) for 30 min at ambient temperature. After 15 min of quenching in PBS-50 mM Tris–HCl (pH 7.5), cells were harvested and extracted with lysis buffer. In addition, cells not treated with DSP were lysed. Lysates were clarified by centrifugation (600 × *g*, 8 min). Fibrinogen was immunoprecipitated by incubating the supernatants overnight at 4 °C with magnetic beads coated with fibrinogen antibodies recognizing Aα, Bβ and γ chains. After washing in PBS containing 0.5 % Triton X-100, immunoprecipitates were boiled in Laemmli's buffer, electrophoresed and after transfer to nitrocellulose, membranes incubated with rabbit anti-Grp78 (BiP, 1:4,000), mouse anti-PDI antibody (1:500), or goat anti-human LC3 antibody (1:300). Afterwards, membranes were washed and incubated overnight at 4 °C with the respective horseradish peroxidase-conjugated secondary antibodies (Jackson ImmunoResearch Laboratories, 1:30,000 for 1 h). Immunoreactive bands were visualized by ECL system (GE Healthcare, Bio-Science).

Western blot

Cells were lysed in lysis buffer and centrifuged at 10,000 × *g* for 10 min. The supernatant was recovered and the pellet was washed in ice-cold PBS and solubilized by sonication in 8 M urea containing Laemmli's buffer on ice. Supernatant and dissolved pellets were adjusted in reducing or non-reducing Laemmli's buffer, resolved by SDS-PAGE, and transferred to nitrocellulose membranes. After blocking in 5 % donkey serum or 5 % skimmed milk in TBS-Tween (20 mM Tris–HCl, pH 7.4, 0.5 M NaCl, 0.1 % Tween 20), membranes were incubated overnight at 4 °C with one of the following primary antibodies: rabbit anti-human fibrinogen antibody reactive with Aα, Bβ and γ chains (1:8,000), goat anti-human LC3 antibody (1:300), rabbit anti-ATG5 antibody (1:2,000), mouse anti-GAPDH antibody (1:4,000), mouse anti-PDI antibody (1:500), rabbit anti-Grp78 (BiP, 1:4,000), or goat anti-EDEM1 (1:250). Afterwards, membranes were washed and incubated with the respective horseradish peroxidase-conjugated secondary antibodies (Jackson ImmunoResearch Laboratories, 1:30,000 for 1 h). Immunoreactive bands were visualized by ECL system (GE Healthcare, Bio-Science).

Immuno-purification of autophagosomes

Cells were treated with vinblastine (50 mM, 2 h) in the presence of ^{35}S methionine-cysteine, washed, mechanically removed in cold PBS and pelleted. Afterwards, cells were disintegrated using a Teflon glass homogenizer (10 mM HEPES, pH 7.5, containing 250 mM sucrose, 1 mM EDTA, and protease inhibitor cocktail). Postnuclear supernatants (1,000 × *g*, 10 min, 4 °C) were equilibrated to 35 % iodixanol (OptiPrep, Sigma), overlaid with 25 % Optiprep solution and covered with homogenization buffer. The microsomal fraction was collected after centrifugation (180,000 × *g* at 4 °C for 3 h) at the buffer and 25 % OptiPrep interface. LC3 vesicles were immuno-isolated from the microsomal fraction using rabbit anti-human LC3 antibodies covalently linked with DSP to protein A-magnetic beads. As control, non-immune rabbit serum was linked to protein A-magnetic beads. After overnight incubation at 4 °C, the beads with the bound LC3 vesicles were solubilized in PBS containing 1 % Triton X-100, 0.5 % deoxycholate, and protease inhibitors. Afterwards, fibrinogen was immunoprecipitated (as described above) and Western blot for LC3 performed.

Confocal immunofluorescence

Cells were grown on precision coverslips (0.17 ± 0.01 mm thickness; Glaswarenfabrik Karl Hecht GmbH & Co KG, Sondheim, Germany) and fed with fresh medium 16 h before experiments. Cells were treated with wortmannin (50 nM) or with 3-methyladenine (10 mM) for 4 h or with trichostatin A (10 mM) and wortmannin in combination. Cells were fixed in freshly prepared 3 % formaldehyde (Fluka, Buchs, Switzerland) and permeabilized with saponin (0.3 %).

For single and double fibrinogen and EDEM1 immunofluorescence, rabbit anti-human fibrinogen Aα chain-specific antibodies (1:100) and goat anti-human EDEM1 antibodies (1:50) were applied for 2 h followed by rinses (2 × 5 min) in PBS containing 1 % bovine serum albumin, and incubation with rhodamine Red-X-conjugated affinity-purified donkey anti-rabbit IgG and DyLight488-conjugated affinity-purified $F(ab)_2$ fragments of donkey anti-goat IgG for 1 h. After rinses, the coverslips were mounted on glass slides with Mowiol.

For double immunofluorescence of fibrinogen and p62/SQSTM1, fibrinogen and NBR1, as well as fibrinogen and LC3, rabbit anti-human fibrinogen Aα chain-specific antibodies (1:100), guinea pig anti-human p62/SQSTM1 antibodies (1:100), mouse monoclonal anti-NBR1 antibodies (1:50), and mouse monoclonal anti-LC3 antibodies (1:100) were applied for 2 h, coverslips washed with PBS containing 1 % bovine serum albumin and incubated with rhodamine Red-X-conjugated affinity-purified donkey anti-rabbit IgG, and either Cy2-conjugated affinity-purified donkey anti-guinea pig IgG or Cy2-conjugated affinity-purified $F(ab)_2$ fragments of donkey anti-mouse IgG, respectively.

For triple confocal immunofluorescence of fibrinogen, p62/SQSTM1 and NBR1, or fibrinogen, EDEM1 and

p62/SQSTM1, as well as fibrinogen, EDEM1 and LC3, coverslips were incubated simultaneously with the respective primary antibodies (see above) for 2 h, followed by rinses (2 × 5 min) with PBS containing 1 % bovine serum albumin and incubation with rhodamine Red-X-conjugated affinity-purified donkey anti-rabbit IgG, Cy2-conjugated affinity-purified donkey anti-mouse IgG and AMCA-conjugated affinity-purified $F(ab)_2$ fragments of donkey anti-guinea pig IgG for 1 h. After rinses, coverslips were mounted on glass slides with Mowiol.

Immunofluorescence was recorded with Leica confocal laser scanning microscopes SP2 or SP5 (Leica, Wetzlar, Germany) using the 63× objective (1.3) or Zeiss LSM 510 (Zeiss, Jena, Germany) using 100× objective (1.4). In multiple immunofluorescence overlays, effects of z-axis pixel shifts were corrected. Colocalization channels were calculated using Meta Imaging Series^R MetaMorph software (Meta Series Software 7.7.0; Molecular Devices, Downingtown, PA, USA) and appear in white in all figures. Quantitative evaluation of the colocalization channels was performed using Meta Imaging Series^R MetaMorph software. Illustrations were generated using Photoshop CS3 (Adobe Systems, Inc.). When used, linear adjustment of contrast or brightness was applied to the entire composite pictures equally. For better visibility in triple confocal immunofluorescence pictures, the original blue AMCA fluorescence was converted into yellow.

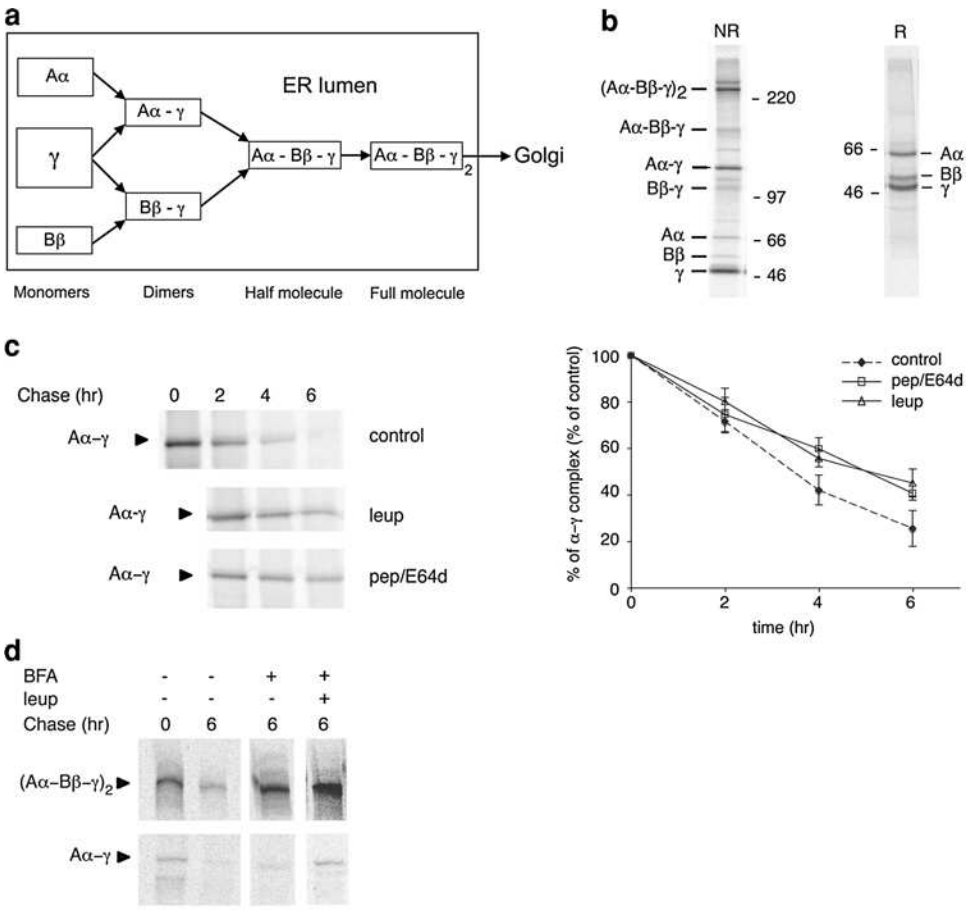

Fig. 1 Degradation of fibrinogen Aα–γ dimers in HepG2 cells is sensitive to lysosomal protease inhibitors in the presence of Brefeldin A. **a** Schematic illustration of the steps of fibrinogen assembly. Full fibrinogen molecules are assembled in the ER from single-chain molecules basically via Bβ–γ dimers. The surplus Aα–γ dimers and single γ chains remain in the ER and become degraded. **b** Western blot for fibrinogen under non-reducing (*NR*, 4–10 % SDS-PAGE) and reducing (*R*, 7.5 % SDS-PAGE) electrophoresis conditions demonstrates non-stoichiometric single-chain synthesis resulting in surplus Aα–γ dimers and γ chains. **c** Pulse-chase and immunoprecipitation of fibrinogen of HepG2 cells followed by non-reducing SDS-PAGE. *Left* Representative phosphor image scans. *Right* Clearance of Aα–γ dimers was quantified relative to the percentage of control and was sensitive to leupeptin and pepstatin/E64D. Data obtained from three independent experiments with bars indicating mean ± SD. **d** Pulse-chase and immunoprecipitation as in **c**. Fibrinogen Aα–γ dimers were degraded in presence of Brefeldin A but accumulated when leupeptin was added. Mature fibrinogen also accumulated in Brefeldin A-treated cells since its transport to the Golgi apparatus and secretion was inhibited by Brefeldin A

Immunoelectron microscopy

HepG2 cells grown to near confluence were fixed in a mixture of 2 % formaldehyde-0.1 % glutaraldehyde in 0.1 M cacodylate buffer (pH 7.2) for 30 min at initially 37 °C, rinsed with buffer, enclosed in 15 % gelatin, infiltrated stepwise with 0.6 M, 1.2 M, and 2.3 M sucrose and frozen in liquid nitrogen. Frozen ultrathin sections were prepared at −110 °C according to Tokuyasu [45, 46]. Before immunolabeling, sections attached to nickel grids were incubated with 2 % gelatine in PBS at 40 °C for 20 min, rinsed with PBS followed by amidination of aldehyde groups with 50 mM NH_4Cl on ice [47]. Ultrathin frozen sections were incubated with fibrinogen Aα chain-specific antibodies (1:50) diluted in PBS containing 1 % BSA and 0.01 % Tween 20 for 2 h followed by several rinses in PBS and 8-nm protein A-gold [43] diluted to an absorbance of 0.1 at 520 nm in PBS containing 1 % bovine serum albumin (or 0.2 % skimmed milk) and 0.01 % Tween 20 for 1 h. After rinses in PBS and finally one rinse in distilled water, sections were postfixed with 1 % glutaraldehyde for 5 min and embedded in 2 % methylcellulose containing 0.3 % uranyl acetate.

For double-immunogold labeling, ultrathin frozen sections were simultaneously incubated with fibrinogen Aα chain specific antibodies (1:50) and antibodies against p62/SQSTM1 (1:25) or NBR1 (1:5) for 2 h, washed with buffer and incubated simultaneously with 12 nm gold-labeled goat anti-rabbit IgG (diluted to an absorbance of 0.1 at 520 nm) and either 6 nm gold-labeled goat anti-guinea pig IgG or 6 nm gold-labeled goat anti-mouse IgG (each diluted to an absorbance of 0.065 at 520 nm) for 1 h followed by rinses, postfixation and methylcellulose/uranyl acetate embedding as described above. For double-immunogold labeling of EDEM1 and fibrinogen (with Aα chain specific antibodies), 12-nm donkey anti-goat IgG and 6-nm donkey anti-rabbit IgG were used as described above.

For pre-embedding immunoperoxidase labeling, cells were grown on coverslips, fixed in situ with 3 % formaldehyde (see above) and permeabilized with 0.05 % saponin followed by incubation with fibrinogen Aα chain-specific antibodies. After rinses with PBS and incubation with horseradish peroxidase-conjugated Fab_2 goat anti-rabbit IgG (4 μg/ml in 1 % BSA-PBS), the diaminobenzidine reaction was performed as described [1]. Serial ultrathin sections from Epon-Araldite embedded cells were prepared in the plane of the cell monolayer.

Sections were observed in a Zeiss 912AB or a Hitachi H-7650 electron microscope at 80 kV and pictures were taken with 70-mm film sheets or a 11-megapixel CCD XR611-M digital camera (Advanced Microscopy Techniques, Woburn, MA, USA). Pictures were generated using Photoshop (Adobe Systems, Inc.) and linear adjustment of contrast or brightness was applied.

Fig. 2 Fibrinogen Aα–γ dimers exit the ER in vesicles. **a–c** Confocal double immunofluorescence for fibrinogen Aα–γ dimers as detected by an Aα chain specific antibody (**a**) and for EDEM1 (**b**) in HepG2 cells. Colocalization channels (**c**) were calculated using Meta Imaging Series^R MetaMorph software. Confocal images are single equatorial optical sections. Boxed fields are shown at higher magnification in the insets. Pictures representative of >50 analyzed cells. *Bar* 10 μm. **d–f** Double-immunogold labeling for fibrinogen (*small gold particles*) and EDEM1 (*large gold particles*, *arrows* in **d**, **e**) shows their close spatial relationship in the ER lumen and presence in a smooth vesicle (**f**, *arrowheads* point to the vesicle membrane). *Bars* 250 nm. **g** Immunoprecipitated fibrinogen from cell lysates was analyzed by Western blotting and representative ECL images are shown. *Left* Immunoprecipitates (IP) contained de-glycosylated EDEM1 (*arrow*) and BiP. *Right* Following protein cross-linking with DSP, both de-glycosylated (*arrow*) and glycosylated (*arrowhead*) EDEM1 were detectable. BiP and to a lesser amount PDI was also found in the immunoprecipitate. DSP protein cross-linking additionally revealed fibrinogen and EDEM1 in high molecular mass bands (*asterisk*). **h** and **i** Membrane buds (marked by a *broken line*) at tips of rough ER cisternae in ultrathin resin (**e**) and frozen sections (**f**) of HepG2 cells. *Bars* 250 nm. **j–m** Immunogold labeling of ultrathin frozen sections for fibrinogen Aα–γ dimers. Gold particles are present in buds at tips of rough ER cisternae (marked by a *broken line* in **j** and **l**) and vesicles of about 150 nm in diameter (**m**). *Bars* 200 nm. **o**, **p** Pre-embedding immunoperoxidase labeling for fibrinogen Aα–γ dimers. Positive DAB reaction (*black*) in an ER bud (*arrowhead* in **o**) and vesicle (*arrowhead* in **p**). *Bars* 200 nm

Serial ultrathin section electron microscopy

HepG2 cells grown to near confluence were fixed in a mixture of 2 % formaldehyde-0.1 % glutaraldehyde in 0.1 M cacodylate buffer (pH 7.2) for 30 min at initially 37 °C, rinsed in buffer and postfixed with 1 % osmium tetroxide in 0.1 M cacodylate buffer (pH 7.2) for 30 min followed by en bloc staining with 1 % aqueous uranyl acetate. After dehydrated in a series of graded ethanol, embedding in Epon-Araldite was performed according to standard protocol. Serial ultrathin sections were cut, ribbons of sections placed on copper slot grids, stained with lead citrate and uranyl acetate and observed with a Hitachi H-7650 electron microscope at 80 kV.

Results

Degradation of fibrinogen Aα–γ dimers occurs in pre-Golgi structures

As mentioned in the Introduction, hepatocytes synthesize unequal amounts of the three different fibrinogen chains and surplus single γ chains become ubiquitinated, which is followed by their proteasomal degradation [25, 26]. However, the clearance mechanism of the surplus Aα–γ dimeric assembly intermediates, which do not become secreted, is unknown. It should be noted that fibrinogen Aα–γ dimers present in the ER are covalently linked by several interchain

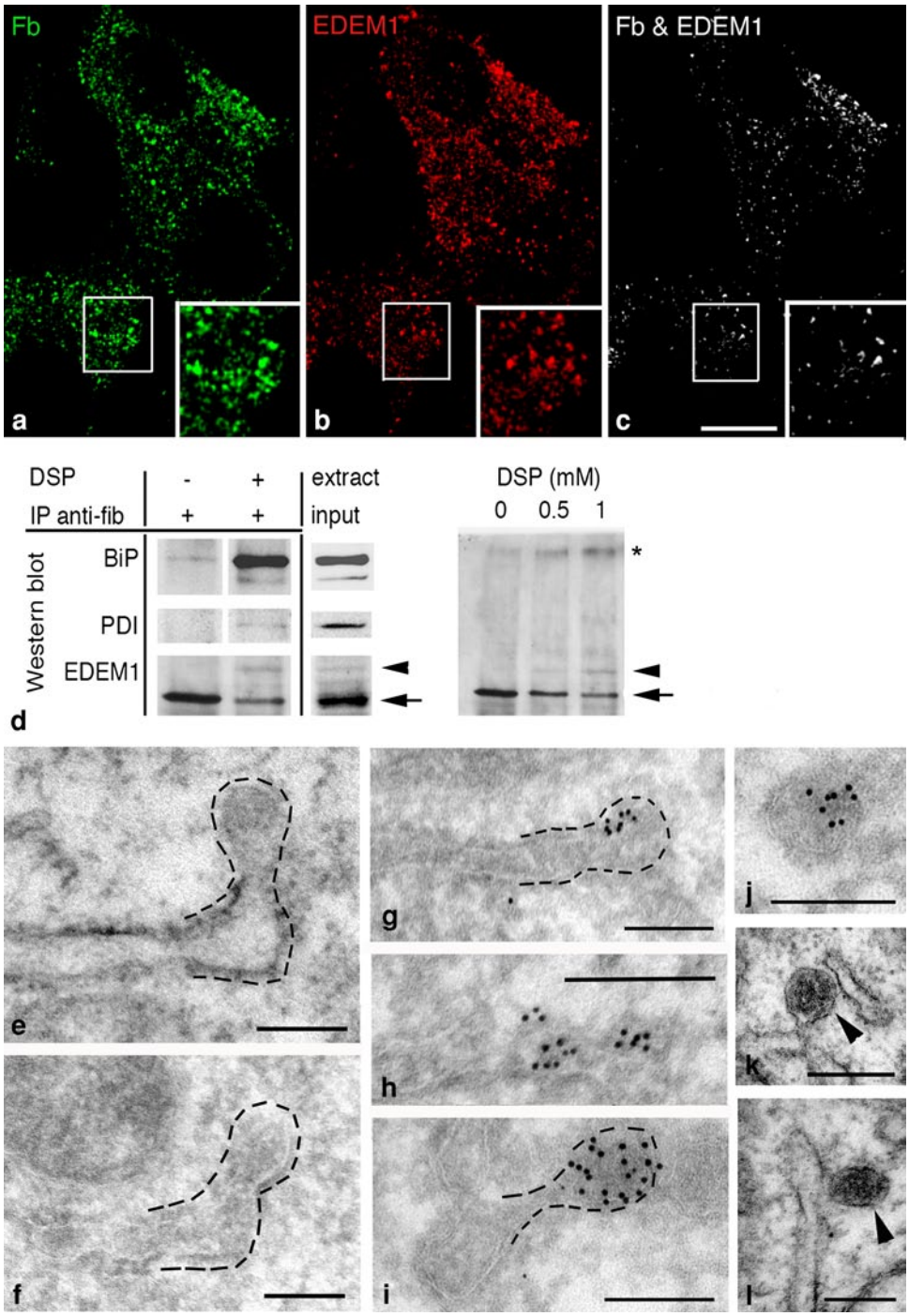

disulfide bonds [7, 12–14]. To analyze the degradation of surplus fibrinogen Aα–γ dimers, we took advantage of HepG2 cells, which synthesize unequal amounts of fibrinogen chains. Figure 1a is a schematic presentation of the assembly pathway to mature fibrinogen that begins with the formation of two types of fibrinogen dimers followed by the formation of a fibrinogen trimer and the fully assembled fibrinogen molecule. Western blots of lysates from resting HepG2 cells, which were resolved by gel electrophoresis under non-reducing conditions, demonstrated γ chains as the dominant species of single chains and Aα–γ dimers as the most abundant dimer of fibrinogen (Fig. 1b, left panel). Western blots from lysates resolved under reducing conditions of gel electrophoresis confirmed the abundance of γ chains and showed that Bβ chains constituted the least abundant and, therefore, rate-limiting single-chain species (Fig. 1b, right panel). Although it has been shown that surplus single γ chains are degraded by proteasomes [25, 26;

see also Supplemental Fig. 1], proteasome inhibitors such as MG132, ALLN, and lactacystin had no effect on fibrinogen Aα–γ dimer turnover (Supplemental Fig. 1). However, the turnover of fibrinogen Aα–γ dimers was partially sensitive to leupeptin and pepstatin A/E64d (Fig. 1c), demonstrating the involvement of lysosomal protease activity. Notably, in HepG2 cells treated with Brefeldin A, degradation of fibrinogen Aα–γ dimers remained sensitive to leupeptin (Fig. 1d). This demonstrated their ongoing degradation after Brefeldin A-induced Golgi apparatus disassembly and disruption of ER-to-Golgi transport. Together, these data excluded the classical lysosomal pathway for the degradation of fibrinogen Aα–γ dimers and indicated the involvement of pre-Golgi structures for the dislocation to their site of degradation. Based on these observations, we found it tempting to investigate whether fibrinogen Aα–γ dimers are removed by the EDEM1 vesicular ER exit pathway [1].

Fibrinogen Aα–γ dimers exit the ER in vesicles

To investigate the possible relationship between fibrinogen and EDEM1, a combined microscopic and biochemical analysis was performed. By double-confocal immunofluorescence, fibrinogen Aα–γ dimers as detected by an Aα chain-specific antibody exhibited a fine reticular and a punctate staining pattern (Fig. 2a), whereas EDEM1 staining was punctate throughout the cytoplasm (Fig. 2b; see also [1, 41]). Fibrinogen and EDEM1 colocalized in spots of different sizes (Fig. 2c). High-resolution double-immunogold labeling directly demonstrated the presence of both fibrinogen and EDEM1 in small regions of the lumen of some ER cisternae (Fig. 2d, e). This was in agreement with our previous results showing the presence of EDEM1 in limited parts of some ER cisternae (see Figs. 3k1–k4 and Figs. 4 d1-d4 in [1], and Fig. 7.3 and 7.4 in [41]. In addition, smooth vesicles of ≥150-nm diameter were positive for fibrinogen and EDEM1 by double-immunogold labeling (Fig. 2f), which does not necessarily mean that all fibrinogen-containing vesicles contain EDEM1 and vice versa. The close spatial relationship of fibrinogen Aα–γ dimers and EDEM1 was corroborated by combined immunoprecipitation/Western blot analysis. As shown in Fig. 2g, fibrinogen immunoprecipitates contained EDEM1. When proteins were cross-linked with DSP before fibrinogen immunoprecipitation, the glycosylated and de-glycosylated forms of EDEM1 could be detected (Fig. 2g, left panel) and high molecular mass bands became noticeable indicating the formation of large complexes of fibrinogen and EDEM1 (Fig. 2g, right panel). The fibrinogen immunoprecipitate also contained BiP and protein disulfide isomerase (Fig. 2g, right panel), as previously shown by others [48–50]. Obviously, these were not covalent complexes since their effective detection required protein cross-linking and, if it exists, a possible interaction between fibrinogen Aα–γ dimers and EDEM1 remains to be more directly shown and characterized.

The mechanism of ER-to-cytoplasm dislocation of misfolded luminal glycoproteins is well established and occurs through a hydrophilic conduit composed of the ubiquitin-ligase Hrd1 complex [6, 23, 27, 28, 51]. Much less, however, is known about the location of the ERAD-L dislocation sites and whether they comprise ER microdomains or some particular structures. Our previous study of the ERAD component EDEM1 showed that it becomes sequestered in ER-derived vesicles [1] formed outside of the transitional ER from where COPII-coated vesicles originate [38, 52, 53]. To investigate whether this pathway operates in the dislocation of fibrinogen Aα–γ dimers, high-resolution electron microscopy and immunoelectron microscopy was performed. At tips and in flat parts of simple rough ER cisternae, smooth membrane buds were observed (Figs. 2h, i, 3a–c), which contained fibrinogen as demonstrated by immunogold labeling of ultrathin frozen sections (Fig. 2g–i) and by pre-embedding immunoperoxidase electron microscopy (Fig. 2o). In addition, fibrinogen-containing smooth vesicles close to the rough ER were observed (Fig. 2m, p). Such smooth vesicles were also detected in conventional resin-embedded cells (Fig. 3d–f) and by thorough analysis of ultrathin serial sections (Fig. 3g–k). These vesicles contained an electron-dense material, which is indicative of high protein content. As revealed in fortuitous ultrathin serial sections (Fig. 3l–n), these ER buds are different from COPII-coated buds of transitional ER representing the canonical ER exit sites for transport to the Golgi apparatus [52, 54]. We noticed that equatorially sectioned smooth vesicles may lack part of their limiting membrane (Fig. 3f, i, arrowheads) whereby their content becomes exposed to the cytosol. This finding is of importance for the mechanism of the autophagic clearance of fibrinogen Aα–γ dimers, which we will report below.

Taken together, our results show that not only EDEM1 [1] but also naturally occurring surplus fibrinogen Aα–γ assembly intermediates exit the ER in non-COPII vesicles. As mentioned above, the vesicular ER exit of EDEM1 is followed by its autophagic degradation [41, 42]. In view of this and the finding that degradation of surplus fibrinogen Aα–γ assembly intermediates is not sensitive to proteasome inhibition (Supplemental Fig. 1) and occurs from pre-Golgi structures (Fig. 1c, d), we decided to focus on autophagy as the possible degradation mechanism of surplus fibrinogen Aα–γ assembly intermediates.

Cytoplasmic fibrinogen Aα–γ dimers are degraded by autophagy

Autophagy represents a major cellular degradation system for cell-own components and is important for cellular

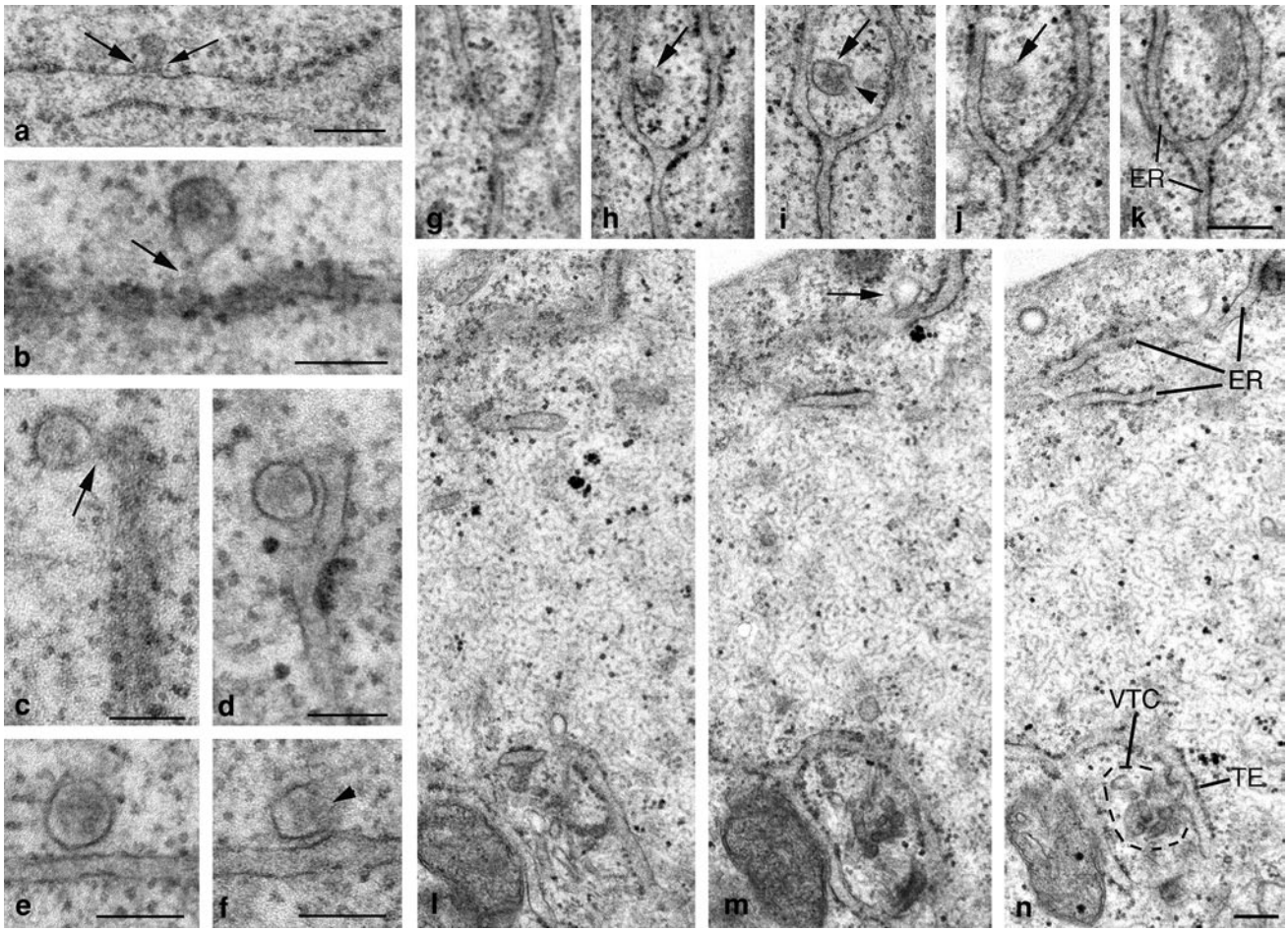

Fig. 3 Budding profiles and non-coated vesicles exist along simple rough ER cisternae. **a–c** Single membrane buds (*arrows* point to necks) of rough ER cisternae in control HepG2 cells. *Bars* 200 nm. **d–f** Non-coated single vesicles adjacent to ER cisternae. Note the partial absence of vesicle membrane in **f** (*arrowhead*). *Bars* 200 nm. **g–k** Consecutive serial ultrathin sections show a single non-coated vesicle (*arrows* in **h–j**) adjacent to simple ER forming a bifurcation. Note the partial absence of vesicle membrane in **i** (*arrowhead*). *Bar* 200 nm. **l–m** Consecutive serial ultrathin sections showing both a membrane bud at a simple ER cisterna (*arrow* in **m**) and an independent ER exit site composed of transitional ER (TE in **n**) with COPII-coated membrane buds and associated vesiculo-tubular cluster (VTC in **n**). *Bar* 200 nm

homeostasis [55, 56]. Macroautophagy, through which parts of the cytoplasm and different organelles become sequestered and degraded, involves the formation of a double-membrane limited autophagosome from the crescent-shaped isolation membrane, and the subsequent fusion of autophagosomes with lysosomes generates the lytic autolysosomes [57, 58]. A large number of proteins, encoded by autophagy-related genes (*Atg*), are involved in the formation of autophagosomes [56]. Among them, LC3 (microtubule-associated protein 1 light chain 3; ATG8 in yeast) has been shown to be a reliable marker protein for the detection of autophagosomes by immunocytochemistry [59]. By double confocal immunofluorescence using antibodies against LC3, fibrinogen Aα–γ dimers could be detected in autophagosomes of resting HepG2 cells (Fig. 4a–c). Typically, autophagy can be enhanced by nutrient deprivation. When cells were grown in serum-free medium for 1.5 h, they displayed abundant autophagosomes, which were positive for fibrinogen (Fig. 4d–f). To gain further insight into the relation of fibrinogen Aα–γ dimers and EDEM1 during degradation by autophagy, we analyzed their colocalization channels with LC3 by triple confocal immunofluorescence in resting and starved cells. Both fibrinogen Aα–γ dimers and EDEM1 were found to be colocalized (Fig. 4g, see also Fig. 2). As expected, the number of colocalized puncta was increased by 63 % following starvation and more larger-size puncta were obvious (compare Fig. 4g with k). Under both conditions, the population of autophagosomes containing fibrinogen Aα–γ dimers (Fig. 4h, i) was larger than the one containing EDEM1 (Fig. 4l, m). In resting cells, 18.6 ± 0.02 % of total autophagosomes contained fibrinogen Aα–γ dimers, which increased to 37.3 ± 0.08 % in

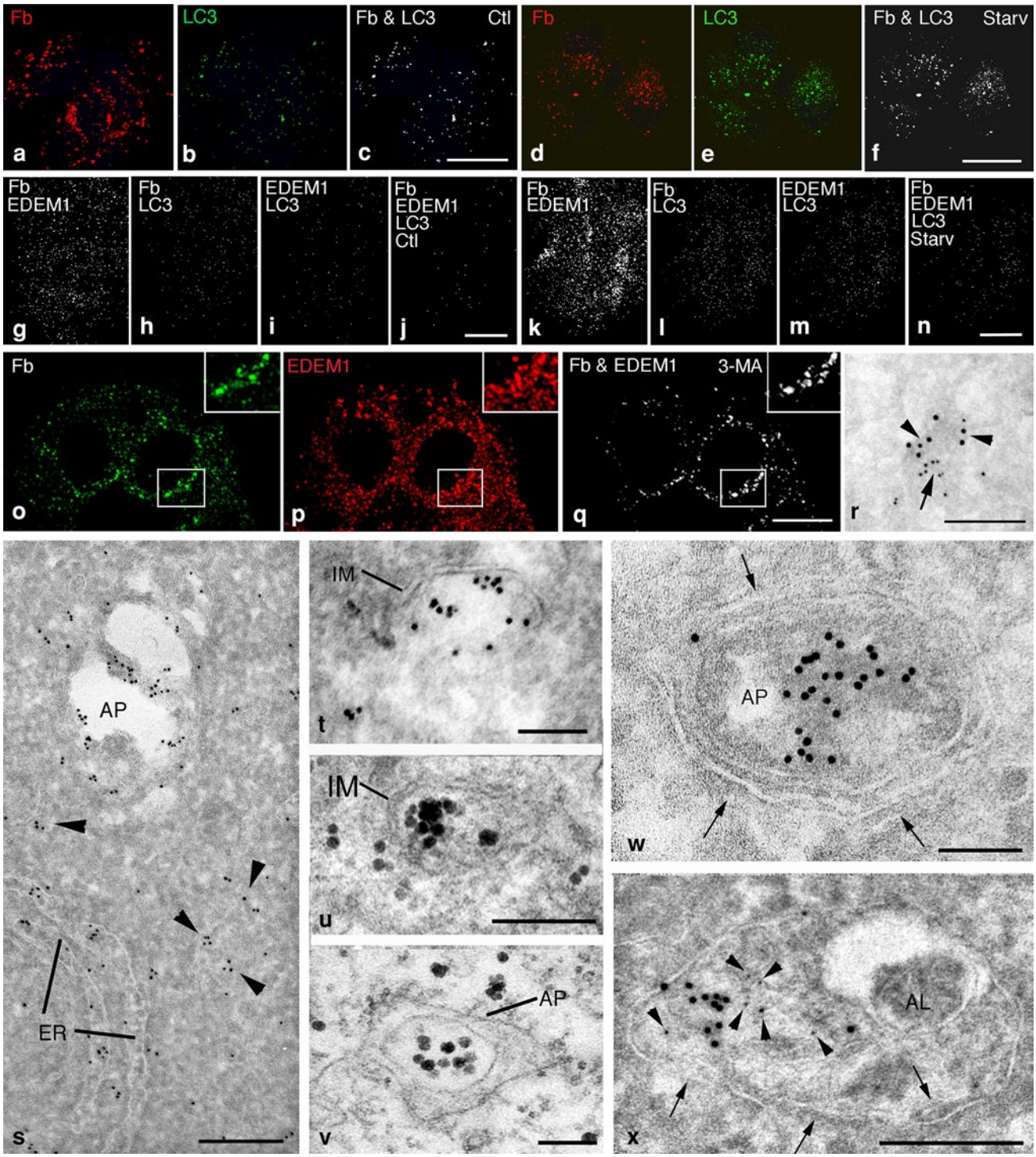

starved cells. Furthermore, in resting cells, 8.9 ± 0.02 % of total autophagosomes contained EDEM1 and this value increased to 15.5 ± 0.07 % in starved cells. Rather few autophagosomes contained both fibrinogen Aα–γ dimers and EDEM1 (2.6 ± 0.008 % in resting and 6.4 ± 3.2 % in starved cells, Fig. 4j, n). These results clearly show how heterogenous the population of autophagosomes is in regard to their content for fibrinogen Aα–γ dimers or EDEM1. This is in agreement with the variable colocalization of fibrinogen Aα–γ dimers with two different selective autophagy cargo receptors (see below and Figs. 6, 7).

Among the autophagy-related proteins, an autophagy-specific phosphoinositide 3-kinase complex is essential for autophagosome formation [60, 61]. When we treated HepG2

◀**Fig. 4** Fibrinogen Aα–γ dimers are present in autophagosomes. **a**–**f** Double confocal immunofluorescence reveals colocalization of fibrinogen Aα–γ dimers and autophagosome marker LC3 in control (**a**–**c**) and starved (**d**–**f**) cells. Confocal images are top-to-bottom z-stacks representative of >50 analyzed cells. *Bars* 10 μm. **g**–**n** Colocalization channels from triple confocal immunofluorescence for fibrinogen, EDEM1 and LC3 in control (**g**–**j**) and starved (**k**–**n**) cells. Confocal images are top-to-bottom z-stacks. *Bars* 10 μm. **o**–**q** Confocal double immunofluorescence for fibrinogen Aα–γ dimers and EDEM1 in 3-methyladenine-treated HepG2 cells. Colocalization channels show that autophagy inhibition results in numerous large clusters of colocalized fibrinogen and EDEM1. *Boxed fields* are shown at higher magnification in the insets. Confocal images are top-to-bottom z-stacks representative of >50 analyzed cells. *Bar* 10 μm. **r** Double immunogold labeling of ultrathin frozen sections from wortmannin-treated HepG2 cells shows fibrinogen (*large gold particles*, *arrowheads*) and EDEM1 (*small gold particles*, *arrow*) in not membrane limited cytoplasmic cluster. *Bar* 200 nm. **s** Immunogold labeling of ultrathin frozen sections of control cells shows fibrinogen in the ER cisternal lumen, as cytoplasmic clusters (*arrowheads*) and an autophagosome (AP). *Bar* 300 nm. **t**, **u** Cytoplasm immunolabeled for fibrinogen Aα–γ dimers (**t** immunogold; **u**, immunoperoxidase) is engulfed by isolation membrane, an early autophagic structure. *Bars* 100 nm. **v**, **w** Fibrinogen immunolabeling in autophagosomes (AP). *Arrows* point to double membrane of autophagosome. **v** Immunoperoxidase. **w** Immunogold. *Bars* 100 nm. **x** Early autolysosome containing fibrinogen Aα–γ dimers (*large gold particles*) and selective autophagy cargo receptor p62/SQSTM1 (*arrowheads* point to *small gold particles*). Early autolysosomes are only partially limited by a double membrane (*arrows*). *Bars* 250 nm

cells with the phosphoinositide 3-kinase inhibitor 3-methyladenine (3-MA) or wortmannin to inhibit the formation of autophagosomes [60, 62, 63], large clusters of colocalized fibrinogen and EDEM1 were observed in the cytoplasm (Fig. 4o–q and Supplemental Fig. 2). Double immunogold labeling of ultrathin frozen sections from wortmannin-treated cells proved their colocalization (Fig. 4r).

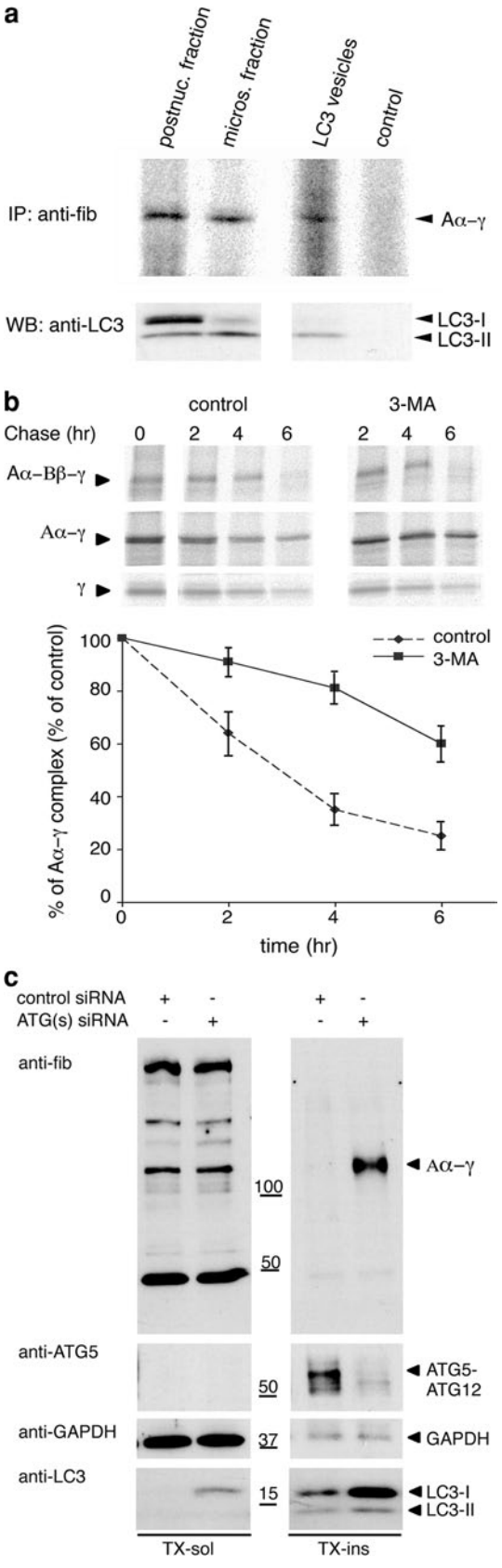

Fig. 5 Fibrinogen Aα–γ dimers are present in autophagosomes ▶ and are degraded by autophagy. **a** *Top* Fibrinogen was immunoprecipitated from postnuclear or microsomal fractions and resolved by non-reducing SDS-PAGE. Autophagosomes (LC3 vesicles) were immuno-isolated with LC3 antibodies from microsomal fractions, fibrinogen immunoprecipitated and resolved by non-reducing SDS-PAGE. In controls, LC3 antibody was replaced by non-immune rabbit serum. *Bottom* Aliquots of immunoprecipitates were probed for LC3 by Western blot and show that the immunopurified LC3 vesicle have only the lipidated, membrane-associated LC3-II. **b** Pulse-chase experiments in presence/absence of 3-methyladenine. Fibrinogen immunoprecipitates were resolved by non-reducing SDS-PAGE. *Top* Representative phosphor image scans. *Bottom* Clearance of Aα–γ dimers was quantified relative to the percentage of control. Data obtained from three independent experiments with bars indicating mean ± SD. **c** siRNA-depletion of *Atg* 5, 7, and 12 and Western blot analysis of Triton X-100 soluble (*left*) and insoluble (*right*) proteins. Fibrinogen Aα–γ dimers accumulate in the Triton X-100 insoluble fraction following siRNA *Atg* knock down

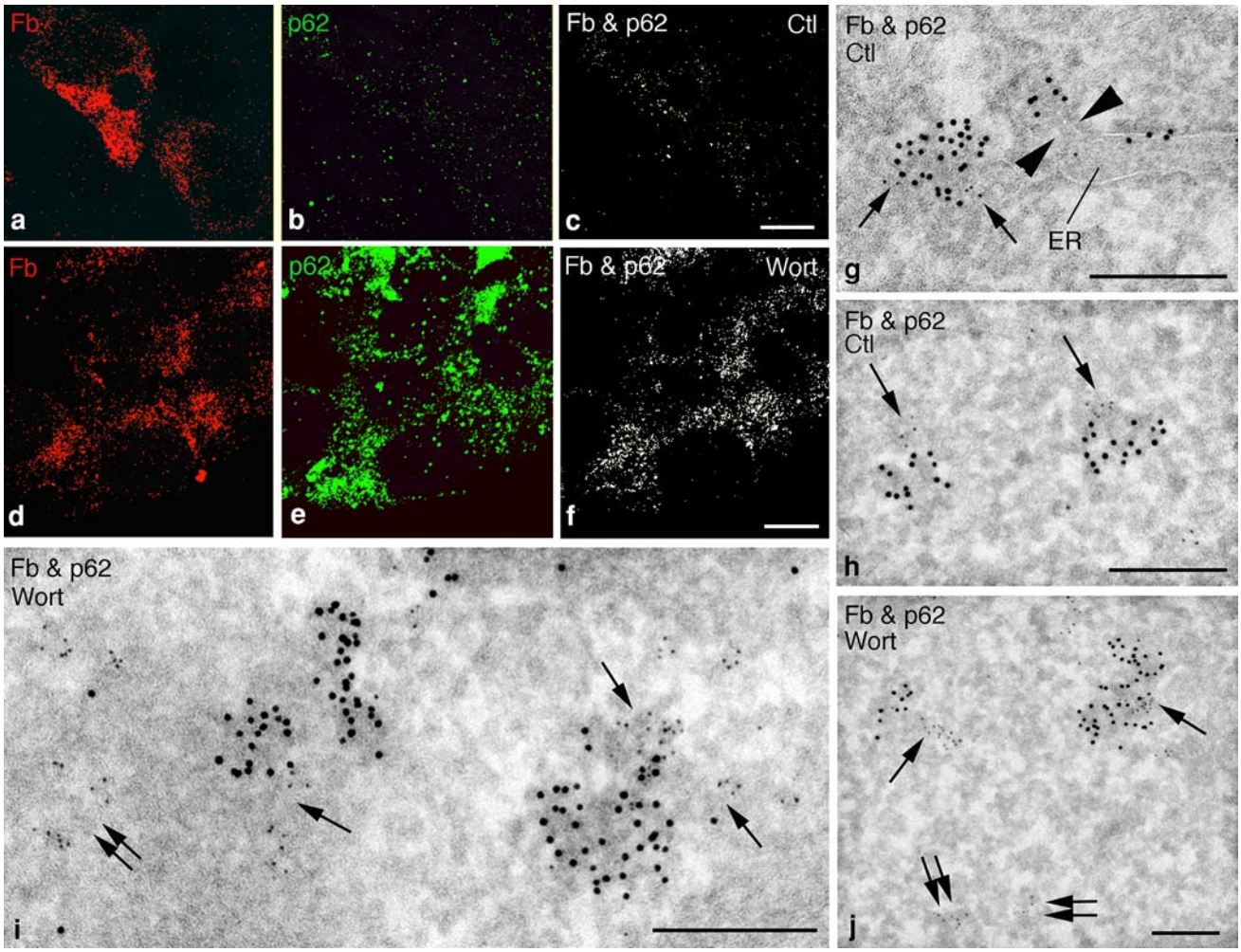

Fig. 6 Fibrinogen Aα–γ dimers and selective autophagy cargo receptor p62/SQSTM1 form aggregates. **a**–**f** Double confocal immunofluorescence reveals colocalization of fibrinogen Aα–γ dimers and p62/SQSTM1 in control (**a**–**c**) and wortmannin-treated (**d**–**f**) HepG2 cells. Confocal images are top-to-bottom z-stacks representative of >50 analyzed cells. **g**–**j** Double-immunogold labeling of ultrathin frozen sections demonstrates cytoplasmic aggregates composed of fibrinogen Aα–γ dimers (*large gold particles*) and p62/SQSTM1 (*small gold particles*, *single arrows*) in control (**g**, **h**) and wortmannin-treated (**i**, **j**) cells. *Double arrows* point to single p62/SQSTM1 labeling. In **g**, an ER cisterna (ER) exhibits a fibrinogen-positive bud (*arrowheads*) and a fibrinogen and p62/SQSTM1-positive aggregate is in the neighboring cytoplasm. *Bars* 10 μm (**a**–**f**); 200 nm (**g**–**j**)

Next, we analyzed the fate of the cytoplasmic fibrinogen Aα–γ dimer clusters by immunoelectron microscopy. Structural hallmarks of autophagy that can be unequivocally identified by transmission electron microscopy are isolation membranes and autophagosomes [57, 58]. The crescent-shaped isolation membranes engulf part of the cytoplasm and/or organelles and through membrane growth and closure mature in autophagosomes, which upon fusion with lysosomes become autolysosomes. In control HepG2 cells, fibrinogen-immunolabeled parts of the cytoplasm were found to be engulfed by isolation membranes (Fig. 4t, u). In addition, typical autophagosomes were also intensely labeled for fibrinogen (Fig. 4s, v, w). Early autolysosomes, which are characteristically surrounded partially by a double and a single membrane [57], contained both fibrinogen Aα–γ dimers and the selective autophagy cargo receptor p62/SQSTM1 as shown by double immunogold labeling (Fig. 4x). Details about the relation of fibrinogen Aα–γ dimers and selective autophagy cargo receptors will be provided below.

The presence of fibrinogen Aα–γ dimers in autophagosomes as shown by immunoelectron microscopy, was independently verified in several biochemical experiments. First, we analyzed the content of LC3 vesicles (autophagosomes) immuno-purified from microsomal fractions of HepG2 cells treated with vinblastine to increase the number of autophagosomes [64]. Western blot analysis of purified autophagosomes resolved under non-reducing conditions of gel electrophoresis showed that they contain fibrinogen Aα–γ dimers (Fig. 5a). As expected, the

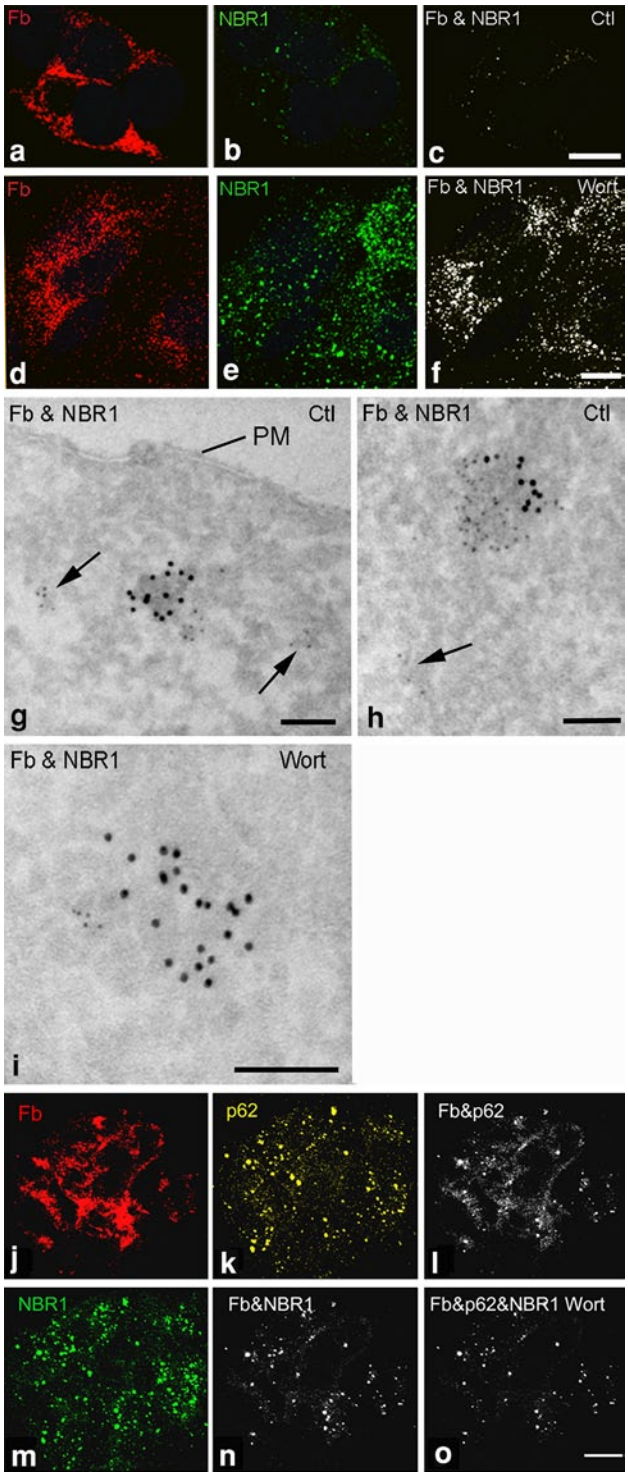

◀ **Fig. 7** Fibrinogen Aα–γ dimers and selective autophagy cargo receptor NBR1 form aggregates. **a–f** Double confocal immunofluorescence reveals colocalization of fibrinogen Aα–γ dimers and NBR1 in control (**a–c**) and wortmannin-treated (**d–f**) HepG2 cells. Confocal images are top-to-bottom z-stacks representative of >50 analyzed cells. **g–i** Double immunogold labeling of ultrathin frozen sections demonstrates cytoplasmic aggregates composed of fibrinogen Aα–γ dimers (*large gold particles*) and NBR1 (*small gold particles*) in control cells. *Double arrows* indicate single NBR1 labeling. **j–o** Triple confocal immunofluorescence demonstrates fibrinogen Aα–γ dimers in p62/SQSTM1 and NBR1 puncta in wortmannin-treated cells. Confocal images are top-to-bottom z-stacks representative of >50 analyzed cells. *Bars* 20 μm (**a–f** and **j–o**); 200 nm (**g–i**)

purified autophagosomes were only positive for LC3-II, the lipidated, membrane-anchored form of LC3. Likewise, our previous work has demonstrated the presence of both EDEM1 and of the lipidated LC3-II form in immuno-purified autophagosomes as well as in EDEM1 vesicle containing fractions of post-nuclear cellular membranes resolved in density gradients [41]. This is in contrast to findings of an association of LC3-I, the cytosolic form LC3, with EDEM1 vesicles in mouse embryo fibroblast [42] and deserves further investigation. In additional pulse-chase experiments, we found that inhibition of autophagy by 3-MA had a strong inhibitory effect on the clearance of fibrinogen Aα–γ dimers, but none on Aα–Bβ–γ half molecules and only little on free γ chains (Fig. 5b). This demonstrates that only fibrinogen Aα–γ dimers are degraded by autophagy. In other experiments, the autophagy-related genes *Atg5*, *Atg7*, and *Atg12* [56] were simultaneously targeted by small interfering RNA. Under these conditions, fibrinogen Aα–γ dimers accumulated in the Triton X-100 insoluble fraction (Fig. 5c, right panel). This was consistent with our earlier observation that detergent-insoluble EDEM1 accumulated after siRNA-mediated inhibition of autophagy [41]. The *Atg* knockdown affected only the clearance of the fibrinogen Aα–γ dimers and had no effect on the fibrinogen assembly (Fig. 5c, left panel). We believe that the fibrinogen Aα–γ dimers detected in the detergent-insoluble fraction correspond to the fibrinogen Aα–γ dimer clusters observed by immunogold electron microscopy (Fig. 4j, k). Obviously, because of their large size, the cytosolic aggregates of fibrinogen Aα–γ dimers cannot be a substrate for proteasomes (see also Supplemental Fig. 1) and are cleared by autophagy.

Although autophagy is generally considered to be unselective, over the recent years it has become obvious that it can also be a selective process [65]. In particular, cytosolic aggregates of misfolded proteins are cleared by selective autophagy, and cargo receptors such as p62/SQSTM1 (sequestosome1) and NBR1 (neighbor of BRCA1 gene 1) provide the specific link to LC3 of autophagosomes [65–68]. Therefore, as a logical next step, we investigated whether cytosolic clusters of fibrinogen Aα–γ dimers were associated with p62/SQSTM1 and NBR1.

Fibrinogen Aα–γ dimers and selective autophagy cargo receptors aggregate in the cytoplasm

To determine the importance of selective autophagy for the removal of fibrinogen Aα–γ dimers, the selective autophagy cargo receptors p62/SQSTM1 and NBR1 [65,

68] were directly investigated by immunocytochemistry. Double confocal immunofluorescence demonstrated colocalization of fibrinogen with p62/SQSTM1 (Fig. 6a–c) and with NBR1 (Fig. 7a–c) in control HepG2 cells. Not unexpected, p62/SQSTM1 and NBR1 puncta outnumbered fibrinogen puncta (see also Figs. 6i, j, 7g, h). Following wortmannin treatment to block autophagy, the number of colocalized fibrinogen and p62/SQSTM1 puncta (Fig. 6 d–f) and of colocalized fibrinogen and NBR1 (Fig. 7d-f) was strongly increased and many larger size puncta were visible. Triple confocal immunofluorescence demonstrated puncta composed of fibrinogen, p62/SQSTM1, and NBR1 (Fig. 7j–o). By high-resolution double-immunogold labeling, fibrinogen and p62/SQSTM1 or NBR1 colocalized in non-membrane bounded cytoplasmic clusters, either close to the ER (Fig. 6g) or dispersed in the cytoplasm in control cells (Figs. 6h, 7g, h) and in wortmannin-treated cells (Figs. 6i, j, 7i). The result shown in Fig. 6g is remarkable since it reveals immunogold labeling for fibrinogen not only in the rough ER lumen and in a smooth bud at the tip of this ER cisterna but additionally in a cytoplasmic cluster, which is also positive for p62/SQSTM1. Such clusters are cleared by selective autophagy as shown by their presence in early autolysosomes (Fig. 4p). However, surprisingly, as the cytoplasmic fibrinogen clusters (Fig. 4s–u), neither the fibrinogen-p62/SQSTM1 nor the fibrinogen-NBR1 clusters were surrounded by a membrane. These results together with our electron microscopic findings of lack of vesicle membranes (Fig. 3f, i) show that the membrane of the ER-derived vesicles becomes dissolved. The mechanism through which this occurs is enigmatic at current and the main focus of ongoing studies in our laboratory.

The formation of large cytoplasmic inclusion bodies composed of misfolded proteins, named aggresomes [69], depends on transport along microtubules by the histone deacetylase-6 (HDAC6)-dynein transport system [70]. However, inhibition of HDAC6 by trichostatin A, a broad spectrum inhibitor of HDACs [71], did not prevent the wortmannin-induced formation of large aggregates of fibrinogen with p62/SQSTM1 or NBR1 (Supplemental Fig. 3), indicating a stochastic process. It should be also remarked that the multiple fibrinogen, p62/SQSTM1 and NBR1 aggregates were always dispersed in the cytoplasm, in contrast to the known pericentrosomal location of single aggresomes [69].

Discussion

We have unraveled the ER-to-cytoplasm dislocation and degradation pathway of the naturally occurring surplus fibrinogen Aα–γ assembly intermediate, which is an ER-retained large protein complex linked by interchain disulfide bonds. Its route comprises vesicular exit from ER cisternae unrelated to the transitional ER of the canonical ER-to-Golgi apparatus exit sites [52, 54]. ER exit is followed by targeting and aggregate formation with the selective autophagy cargo receptors p62/SQSTM1 and NBR1 [65, 72] and the eventual degradation of the protein aggregates by selective autophagy. This new pathway is different from and occurs in parallel to the dislocation and degradation of not secreted surplus fibrinogen γ chains (Fig. 8).

The degradation of surplus single fibrinogen γ chains bears similarities with ERAD-L of misfolded luminal glycoproteins such as mutant carboxypeptidase Y (CPY*) in yeast [2, 27, 73] and Null Hong Kong variant

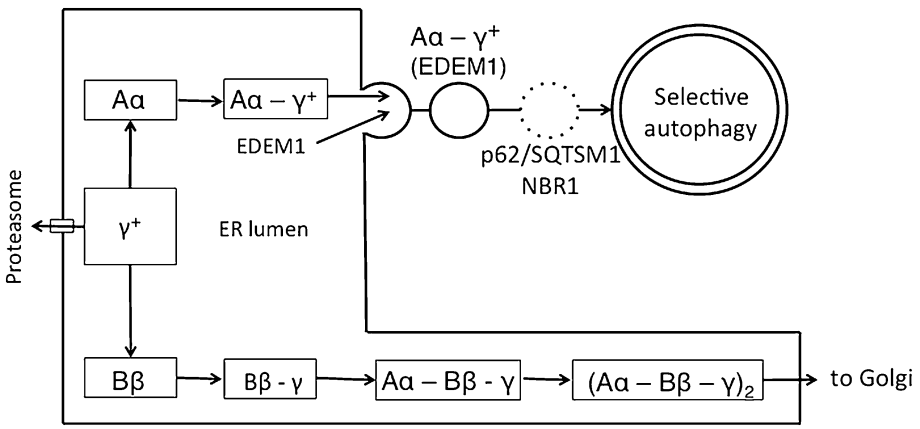

Fig. 8 Summary of destinies of fibrinogen assembly components. Surplus fibrinogen Aα–γ dimers (Aα–γ^+) and EDEM1 egress from the ER to the cytoplasm through a vesicular pathway. Following the dissolution of the vesicle membrane through a currently unknown mechanism, the surplus fibrinogen Aα–γ dimers (Aα–γ^+) become target for the selective autophagy cargo receptors p62/SQSTM1 and NBR1, and are degraded by selective autophagy as shown in the present study. Surplus single γ chains (γ^+) undergo proteasomal degradation as shown by others [25, 26]. Full molecules exit to the Golgi apparatus

of α1-antitrypsin in mammalian cells [74, 75] in so far that they become degraded by the ubiquitin–proteasome system. In contrast, surplus fibrinogen Aα–γ assembly intermediates pursue a different route, which involves their vesicular dislocation to the cytoplasm. How can this possibly be explained? Obviously, single-chain luminal proteins in the native or misfolded state can be dislocated through the postulated hydrophilic pore formed by the ubiquitin-ligase Hrd1 complex [23, 24]. Currently, the crystal structure of ubiquitin-ligase Hrd1p is not known and hence the size of its postulated hydrophilic pore has not been determined. However, it might well be comparable to the size of the pore of the Sec61 translocon, which ranges dynamically between 4 and 24 Å [76–78]. The molecular mass of a fibrinogen Aα–γ dimer is about 125 kD and that does not account for the *N*-linked high mannose-type oligosaccharide at Asn 52 of the γ chain. Thus, fibrinogen single γ chains and, for instance, misfolded α1-antitrypsin are of considerable lower molecular mass and size than the fibrinogen Aα–γ assembly intermediate. When considering the dimension of the fibrinogen Aα–γ dimer, its three symmetrical disulfide interchain bonds [12] have been shown to contribute to the formation of the central globular E domain, which is about 50 Å in diameter in the fibrinogen molecule [79, 80]. The lateral D domain of fibrinogen, which is about 65 Å in diameter, contains the C-terminal part of the Aα and γ chains from which the Aα chain extends [79, 81]. Although information about the exact dimension of surplus fibrinogen Aα–γ dimers as they exist in the ER lumen is not available, it seems reasonable to consider that because of their large size and possible interaction with other proteins such as EDEM1, their dislocation to the cytoplasm may require a means different from the ubiquitin-ligase Hrd1p complex. As shown in the present study, their dislocation to the cytoplasm involves sequestration in ER membrane buds lacking a recognizable cytosolic coat, which pinch-off to form ≥150-nm vesicles. By all means, these vesicles seem to correspond to the ER-derived vesicles we have discovered during the course of our studies on EDEM1 [1] and which are obviously different from the COPII-coated vesicles derived from the transitional ER [38, 52]. Our detailed comparative electron microscopic analysis unequivocally establishes that vesicle formation not only occurs at the transitional ER but also along simple ER cisternae. These vesicles, which lack a cytosolic COPII coat, are larger than standard 60–90-nm COPII vesicles and different from the long tubular COPII carriers transporting bulky cargo such as procollagen fibrils from the transitional ER to the Golgi apparatus [82, 83].

Is it possible that targets other than fibrinogen Aα–γ dimer assembly intermediates are dislocated to the cytoplasm by this novel vesicular pathway? Actually, there is the classic observation by Palade [84] of intracisternal granules in the ER lumen of acinar pancreatic cells, which were shown later to be composed of aggregated secretory zymogens [85]. Other secretory proteins such as thyroglobulin [86] and immunoglobulins in lymphoid cells [87, 88] aggregate in the ER lumen, which in the case of thyroglobulin involves interchain disulfide bonds and association with BiP [86]. As mentioned, the Null Hong Kong variant of α1-antitrypsin is dislocated by the ubiquitin-ligase Hrd1 complex. In contrast, the PiZ-variant of α1-antitrypsin forms aggregates in the ER [89, 90] that are subsequently degraded by autophagy [91]. The events that precede the autophagic degradation are unknown. In addition, glaucoma-causing mutant misfolded myocilin forms aggregates that are retained in the ER and are not degraded by proteasomes [92]. Hence, the tendency to aggregate in the lumen of the ER of a number of normal and mutant secretory proteins would render them candidates for dislocation by the vesicular exit route.

As shown here, following their dislocation in ER-derived vesicles, fibrinogen Aα–γ dimers exist as cytosolic aggregates together with the selective autophagy cargo receptors p62/SQSTM1 and NBR1, which are both cytosolic proteins [65]. This is not only surprising but also represents a formidable topologic problem. This necessitates that the membrane of the ER-derived fibrinogen Aα–γ containing vesicles becomes dissolved. Indeed, the clusters composed of fibrinogen and p62/SQSTM1 or NBR1 in the cytoplasm were not membrane-limited as unambiguously shown by electron microscopy. The intriguing question of how the membrane of the vesicle becomes dissolved is currently under study in our laboratory. The cytosolic aggregates composed of fibrinogen Aα–γ dimers, p62/SQSTM1, and NBR1 become degraded by selective autophagy since they are unsuitable for proteasomal degradation due to size constraints.

Our findings demonstrate that under basal cellular conditions, different pathways exist in parallel for ER-to-cytoplasm dislocation and subsequent degradation of large luminal protein complexes and of small single-chain proteins. We provide data in support of a novel route for the dislocation to the cytoplasm of ER-retained large protein complexes. This route apparently would also provide an ER exit pathway for particles such as certain viruses, which require components of the ERAD machinery for their transport to the cytoplasm [93, 94]. Together, the dislocation pathway for surplus fibrinogen Aα–γ assembly intermediates reported here furthers our understanding of the different disposal mechanisms cells have developed for different proteins and protein assembly intermediates as well as viruses under physiologic and diseased conditions. In more general terms, the classical view of the ERAD as a disposal pathway for misfolded proteins has to be expanded to also include the elimination of native proteins, whose persistence could be disadvantageous for ER proteostasis.

Acknowledgments We thank W.S. Hancock (Boston, MA), N.-O. Ku (Seoul), P.M. Lackie (Southampton), Jon Sonderholm (Seoul), D.J. Taatjes (Burlington, VT) and G.H.F. Yam (Hong Kong) for critical reading of the manuscript. We are grateful to Tamara Locher and Roger Santimaria for skillful technical assistance. Insook Jang is recipient of a fellowship from the Brain Korea 21 program. Funding was received by the Swiss National Science Foundation (to J.R.), the Canton of Zurich (to J.R.), by the World Class University Program through the National Research Foundation of Korea funded by the Ministry of Education, Science and Technology (R31-2008-000-10086-0) (to J.R. and J.W.C), the National Research Foundation of Korea by the Ministry of Education, Science and Technology (2010-0027736) (to J.R. and J.W.C) and partly by the National Research Foundation funded by the Korean Government (2012R1A2A1A05026333) (to J.W.C.).

Conflict of interest The authors declare they have no competing interests.

References

1. Zuber C, Cormier JH, Guhl B, Santimaria R, Hebert DN, Roth J (2007) EDEM1 reveals a quality control vesicular transport pathway out of the endoplasmic reticulum not involving the COPII exit sites. Proc Natl Acad Sci USA 104:4407–4412
2. Hiller MM, Finger A, Schweiger M, Wolf DH (1996) ER degradation of a misfolded luminal protein by the cytosolic ubiquitin-proteasome pathway. Science 273:1725–1728
3. Braakman I, Bulleid NJ (2011) Protein folding and modification in the mammalian endoplasmic reticulum. Annu Rev Biochem 80:71–99
4. Bonifacino JS, Weissman AM (1998) Ubiquitin and the control of protein fate in the secretory and endocytic pathways. Annu Rev Cell Dev Biol 14:19–57
5. Christis C, Lubsen N, Braakman I (2008) Protein folding includes oligomerization: examples from the endoplasmic reticulum and cytosol. FEBS J 275:4700–4727
6. Bagola K, Mehnert M, Jarosch E, Sommer T (2011) Protein dislocation from the ER. Biochim Biophys Acta 1808:925–936
7. Weisel JW (2005) Fibrinogen and fibrin. Adv Protein Chem 70:247–299
8. Redman CM, Xia H (2001) Fibrinogen biosynthesis. Assembly, intracellular degradation, and association with lipid synthesis and secretion. Ann NY Acad Sci 936:480–495
9. Mosesson MW, Siebenlist KR, Meh DA (2001) The structure and biological features of fibrinogen and fibrin. Ann NY Acad Sci 936:11–30
10. Yu S, Sher B, Kudryk B, Redman CM (1984) Fibrinogen precursors. Order of assembly of fibrinogen chains. J Biol Chem 259:10574–10581
11. Huang S, Cao Z, Chung DW, Davie EW (1996) The role of beta-gamma and alpha-gamma complexes in the assembly of human fibrinogen. J Biol Chem 271:27942–27947
12. Blomback B, Hessel B, Hogg D (1976) Disulfide bridges in NH2-terminal part of human fibrinogen. Thrombosis Res 8:639–658
13. Huang S, Cao Z, Davie EW (1993) The role of amino-terminal disulfide bonds in the structure and assembly of human fibrinogen. Biochem Biophys Res Commun 190:488–495
14. Henschen A (1978) Disulfide bridges in the middle part of human fibrinogen. Hoppe-Seyler's Z Physiol Chemie 359:1757–1770
15. Walter P, Ron D (2011) The unfolded protein response: from stress pathway to homeostatic regulation. Science 334:1081–1086
16. Yang M, Omura S, Bonifacino JS, Weissman AM (1998) Novel aspects of degradation of T cell receptor subunits from the endoplasmic reticulum (ER) in T cells: importance of oligosaccharide processing, ubiquitination, and proteasome-dependent removal from ER membranes. J Exp Med 187:835–846
17. Huppa JB, Ploegh HL (1997) The alpha chain of the T cell antigen receptor is degraded in the cytosol. Immunity 7:113–122
18. Yu H, Kaung G, Kobayashi S, Kopito RR (1997) Cytosolic degradation of T-cell receptor alpha chains by the proteasome. J Biol Chem 272:20800–20804
19. Bonifacino JS, Suzuki CK, Lippincott-Schwartz J, Weissman AM, Klausner RD (1989) Pre-Golgi degradation of newly synthesized T-cell antigen receptor chains: intrinsic sensitivity and the role of subunit assembly. J Cell Biol 109:73–83
20. Tiwari S, Weissman AM (2001) Endoplasmic reticulum (ER)-associated degradation of T cell receptor subunits. Involvement of ER-associated ubiquitin-conjugating enzymes (E2 s). J Biol Chem 276:16193–16200
21. Bonifacino J, McCarthy S, Maguire J, Nakayama T, Singer D, Klausner R, Singer A (1990) Novel post-translational regulation of TCR expression in CD4+ CD8+ thymocytes influenced by CD4. Nature 344:247–251
22. Kearse K, Roberts J, Munitz T, Wiest D, Nakayama T, Singer A (1994) Developmental regulation of αβ T cell antigen receptor expression results from differential stability of nascent TCR-α proteins within the endoplasmic reticulum of immature and mature T cells. EMBO J 13:4504–4514
23. Carvalho P, Goder V, Rapoport TA (2006) Distinct ubiquitin-ligase complexes define convergent pathways for the degradation of ER proteins. Cell 126:361–373
24. Sato BK, Schulz D, Do PH, Hampton RY (2009) Misfolded membrane proteins are specifically recognized by the transmembrane domain of the Hrd1p ubiquitin ligase. Mol Cell 34: 212–222
25. Roy S, Yu S, Banerjee D, Overton O, Mukhopadhyay G, Oddoux C, Grieninger G, Redman C (1992) Assembly and secretion of fibrinogen. Degradation of individual chains. J Biol Chem 267:23151–23158
26. Xia H, Redman C (1999) The degradation of nascent fibrinogen chains is mediated by the ubiquitin proteasome pathway. Biochem Biophys Res Commun 261:590–597
27. Carvalho P, Stanley AM, Rapoport TA (2010) Retrotranslocation of a misfolded luminal ER protein by the ubiquitin-ligase Hrd1p. Cell 143:579–591
28. Denic V, Quan EM, Weissman JS (2006) A luminal surveillance complex that selects misfolded glycoproteins for ER-associated degradation. Cell 126:349–359
29. Molinari M, Calanca V, Galli C, Lucca P, Paganetti P (2003) Role of EDEM in the release of misfolded glycoproteins from the calnexin cycle. Science 299:1397–1400
30. Oda Y, Hosokawa N, Wada I, Nagata K (2003) EDEM as an acceptor of terminally misfolded glycoproteins released from calnexin. Science 299:1394–1397
31. Cormier JH, Tamura T, Sunryd JC, Hebert DN (2009) EDEM1 recognition and delivery of misfolded proteins to the SEL1L-containing ERAD complex. Mol Cell 34:627–633
32. Gauss R, Kanehara K, Carvalho P, Ng DTW, Aebi M (2011) A complex of Pdi1p and the mannosidase Htm1p initiates clearance of unfolded glycoproteins from the endoplasmic reticulum. Mol Cell 42:782–793
33. Quan EM, Kamiya Y, Kamiya D, Denic V, Weibezahn J, Kato K, Weissman JS (2008) Defining the glycan destruction signal for endoplasmic reticulum-associated degradation. Mol Cell 32:870–877
34. Olivari S, Cali T, Salo KE, Paganetti P, Ruddock LW, Molinari M (2006) EDEM1 regulates ER-associated degradation by accelerating de-mannosylation of folding-defective polypeptides and by inhibiting their covalent aggregation. Biochem Biophys Res Commun 349:1278–1284

35. Hosokawa N, Tremblay LO, Sleno B, Kamiya Y, Wada I, Nagata K, Kato K, Herscovics A (2010) EDEM1 accelerates the trimming of α1,2-linked mannose on the C branch of N-glycans. Glycobiology 20:567–575
36. Clerc S, Hirsch C, Oggier DM, Deprez P, Jakob C, Sommer T, Aebi M (2009) Htm1 protein generates the N-glycan signal for glycoprotein degradation in the endoplasmic reticulum. J Cell Biol 184:159–172
37. Zanetti G, Pahuja KB, Studer S, Shim S, Schekman R (2012) COPII and the regulation of protein sorting in mammals. Nat Cell Biol 14(1):20–28
38. Bannykh SI, Rowe T, Balch WE (1996) The organization of endoplasmic reticulum export complexes. J Cell Biol 135:19–35
39. Strous GJ, Van Kerkhof P, Brok R, Roth J, Brada D (1987) Glucosidase II, a protein of the endoplasmic reticulum with high mannose oligosaccharide chains and a rapid turnover. J Biol Chem 262:3620–3625
40. Wu Y, Termine DJ, Swulius MT, Moremen KW, Sifers RN (2007) Human endoplasmic reticulum mannosidase I is subject to regulated proteolysis. J Biol Chem 282:4841–4849
41. Le Fourn V, Gaplovska-Kysela K, Guhl B, Santimaria R, Zuber C, Roth J (2009) Basal autophagy is involved in the degradation of the ERAD component EDEM1. Cell Mol Life Sci 66: 1434–1445
42. Cali T, Galli C, Olivari S, Molinari M (2008) Segregation and rapid turnover of EDEM1 by an autophagy-like mechanism modulates standard ERAD and folding activities. Biochem Biophys Res Commun 371:405–410
43. Roth J, Bendayan M, Orci L (1978) Ultrastructural localization of intracellular antigens by the use of protein A-gold complex. J Histochem Cytochem 26:1074–1081
44. Roth J (1982) The protein A-gold (pAg) technique—a qualitative and quantitative approach for antigen localization on thin sections. In: Bullock G, Petrusz P (eds) Techniques in immunocytochemistry, vol 1. Academic Press, London, pp 108–133
45. Tokuyasu K (1989) Use of poly(vinylpyrrolidone) and poly(vinyl alcohol) for cryoultramicrotomy. Histochem J 21:163–171
46. Tokuyasu K (1978) A study of positive staining of ultrathin frozen sections. J Ultrastruct Res 63:287–307
47. Roth J, Taatjes DJ, Warhol MJ (1989) Prevention of non-specific interactions of gold-labeled reagents on tissue sections. Histochemistry 92:47–56
48. Hartwig R, Danishefsky KJ (1991) Studies on the assembly and secretion of fibrinogen. J Biol Chem 266:6578–6585
49. Huang S, Mulvihill ER, Farrell DH, Chung DW, Davie EW (1993) Biosynthesis of human fibrinogen. Subunit interactions and potential intermediates in the assembly. J Biol Chem 268:8919–8926
50. Roy S, Sun A, Redman C (1996) In vitro assembly of the component chains of fibrinogen requires endoplasmic reticulum factors. J Biol Chem 271:24544–24550
51. Vashist S, Ng DT (2004) Misfolded proteins are sorted by a sequential checkpoint mechanism of ER quality control. J Cell Biol 165:41–52
52. Palade G (1975) Intracellular aspects of the process of protein biosynthesis. Science 189:347–358
53. Zanetti G, Pahuja KB, Studer S, Shim S, Schekman R (2011) COPII and the regulation of protein sorting in mammals. Nat Cell Biol 14:20–28
54. Bannykh SI, Balch WE (1997) Membrane dynamics at the endoplasmic reticulum-Golgi interface. J Cell Biol 138:1–4
55. Yorimitsu T, Klionsky DJ (2005) Autophagy: molecular machinery for self-eating. Cell Death Differ 12(Suppl 2):1542–1552
56. Mizushima N, Yoshimori T, Ohsumi Y (2011) The role of Atg proteins in autophagosome formation. Annu Rev Cell Dev Biol 27:107–132
57. Eskelinen E-L, Reggiori F, Baba M, Kovacs AL, Seglen PO (2011) Seeing is believing: the impact of electron microscopy on autophagy research. Autophagy 7:935–956
58. Pavelka M, Roth J (2010) Functional ultrastructure. An atlas of tissue biology and pathology, 2nd edn. Springer, Vienna
59. Kabeya Y, Mizushima N, Ueno T, Yamamoto A, Kirisako T, Noda T, Kominami E, Ohsumi Y, Yoshimori T (2000) LC3, a mammalian homologue of yeast Apg8p, is localized in autophagosome membranes after processing. EMBO J 19:5720–5728
60. Petiot A, Ogier-Denis E, Blommaart EF, Meijer AJ, Codogno P (2000) Distinct classes of phosphatidylinositol 3'-kinases are involved in signaling pathways that control macroautophagy in HT-29 cells. J Biol Chem 275:992–998
61. Taguchi-Atarashi N, Hamasaki M, Matsunaga K, Omori H, Ktistakis NT, Yoshimori T, Noda T (2010) Modulation of local PtdIns3P levels by the PI phosphatase MTMR3 regulates constitutive autophagy. Traffic 11:468–478
62. Vlahos CJ, Matter WF, Hui KY, Brown RF (1994) A specific inhibitor of phosphatidylinositol 3-kinase, 2-(4-morpholinyl)-8-phenyl-4H-1-benzopyran-4-one (LY294002). J Biol Chem 269:5241–5248
63. Wu YT, Tan HL, Shui G, Bauvy C, Huang Q, Wenk MR, Ong CN, Codogno P, Shen HM (2010) Dual role of 3-methyladenine in modulation of autophagy via different temporal patterns of inhibition on class I and III phosphoinositide 3-kinase. J Biol Chem 285:10850–10861
64. Kochl R, Hu XW, Chan EY, Tooze SA (2006) Microtubules facilitate autophagosome formation and fusion of autophagosomes with endosomes. Traffic 7:129–145
65. Johansen T, Lamark T (2011) Selective autophagy mediated by autophagic adapter proteins. Autophagy 7:279–296
66. Bjorkoy G, Lamark T, Brech A, Outzen H, Perander M, Overvatn A, Stenmark H, Johansen T (2005) p62/SQSTM1 forms protein aggregates degraded by autophagy and has a protective effect on huntingtin-induced cell death. J Cell Biol 171:603–614
67. Pankiv S, Clausen TH, Lamark T, Brech A, Bruun JA, Outzen H, Overvatn A, Bjorkoy G, Johansen T (2007) p62/SQSTM1 binds directly to Atg8/LC3 to facilitate degradation of ubiquitinated protein aggregates by autophagy. J Biol Chem 282:24131–24145
68. Kirkin V, Lamark T, Johansen T, Dikic I (2009) NBR1 cooperates with p62 in selective autophagy of ubiquitinated targets. Autophagy 5:732–733
69. Johnston JA, Ward CL, Kopito RR (1998) Aggresomes: a cellular response to misfolded proteins. J Cell Biol 143:1883–1898
70. Kawaguchi Y, Kovacs JJ, McLaurin A, Vance JM, Ito A, Yao TP (2003) The deacetylase HDAC6 regulates aggresome formation and cell viability in response to misfolded protein stress. Cell 115:727–738
71. Furumai R, Komatsu Y, Nishino N, Khochbin S, Yoshida M, Horinouchi S (2001) Potent histone deacetylase inhibitors built from trichostatin A and cyclic tetrapeptide antibiotics including trapoxin. Proc Natl Acad Sci USA 98:87–92
72. Kirkin V, Lamark T, Sou YS, Bjorkoy G, Nunn JL, Bruun JA, Shvets E, McEwan DG, Clausen TH, Wild P, Bilusic I, Theurillat JP, Overvatn A, Ishii T, Elazar Z, Komatsu M, Dikic I, Johansen T (2009) A role for NBR1 in autophagosomal degradation of ubiquitinated substrates. Mol Cell 33:505–516
73. Bordallo J, Plemper RK, Finger A, Wolf DH (1998) De3p/Hrd1p is required for endoplasmic reticulum-associated degradation of misfolded lumenal and integral membrane proteins. Mol Biol Cell 9:209–222
74. Werner ED, Brodsky JL, McCracken AA (1996) Proteasome-dependent endoplasmic reticulum-associated protein degradation: an unconventional route to a familiar fate. Proc Natl Acad Sci USA 93:13797–13801

75. Teckman JH, Perlmutter DH (1996) The endoplasmic reticulum degradation pathway for mutant secretory proteins alpha 1-antitrypsin Z and S is distinct from that for an unassembled membrane protein. J Biol Chem 271:13215–13220
76. Osborne AR, Rapoport TA, van den Berg B (2005) Protein translocation by the Sec61/SecY channel. Annu Rev Cell Dev Biol 21:529–550
77. Bonardi F, Halza E, Walko M, Du Plessis Fß, Nouwen N, Feringa BL, Driessen AJM (2011) Probing the SecYEG translocation pore size with preproteins conjugated with sizable rigid spherical molecules. Proc Natl Acad Sci USA 108:7775–7780
78. Tian P, Andricioaei I (2006) Size, motion, and function of the SecY translocon revealed by molecular dynamics simulations with virtual probes. Biophys J 90:2718–2730
79. Yermolenko IS, Lishko VK, Ugarova TP, Magonov SN (2011) High-resolution visualization of fibrinogen molecules and fibrin fibers with atomic force microscopy. Biomacromolecules 12:370–379
80. Kollman JM, Pandi L, Sawaya MR, Riley M, Doolittle RF (2009) Crystal structure of human fibrinogen. Biochemistry 48:3877–3886
81. Mosesson MW, Hainfeld J, Wall J, Haschemeyer RH (1981) Identification and mass analysis of human fibrinogen molecules and their domains by scanning transmission electron microscopy. J Mol Biol 153:695–718
82. Saito K, Yamashiro K, Ichikawa Y, Erlmann P, Kontani K, Malhotra V, Katada T (2011) cTAGE5 mediates collagen secretion through interaction with TANGO1 at endoplasmic reticulum exit sites. Mol Biol Cell 22:2301–2308
83. Malhotra V, Erlmann P (2011) Protein export at the ER: loading big collagens into COPII carriers. EMBO J 30:3475–3480
84. Palade GE (1956) Intracisternal granules in the exocrine cells of the pancreas. J Biophys Biochem Cytol 2:417–422
85. Geuze HJ, Slot JW (1980) Disproportional immunostaining patterns of two secretory proteins in guinea pig and rat exocrine pancreatic cells. An immunoferritin and fluorescence study. Eur J Cell Biol 21:93–100
86. Kim PS, Bole D, Arvan P (1992) Transient aggregation of nascent thyroglobulin in the endoplasmic reticulum: relationship to the molecular chaperone, BiP. J Cell Biol 118:541–549
87. Alanen A, Pira U, Lassila O, Roth J, Franklin RM (1985) Mott cells are plasma cells defective in immunoglobulin secretion. Eur J Immunol 15:235–242
88. Brewer JW, Randall TD, Parkhouse RM, Corley RB (1994) Mechanism and subcellular localization of secretory IgM polymer assembly. J Biol Chem 269:17338–17348
89. Lomas DA, Evans DL, Finch JT, Carrell RW (1992) The mechanism of Z alpha 1-antitrypsin accumulation in the liver. Nature 357:605–607
90. Lin L, Schmidt B, Teckman J, Perlmutter DH (2001) A naturally occurring nonpolymerogenic mutant of alpha 1-antitrypsin characterized by prolonged retention in the endoplasmic reticulum. J Biol Chem 276:33893–33898
91. Kamimoto T, Shoji S, Hidvegi T, Mizushima N, Umebayashi K, Perlmutter DH, Yoshimori T (2006) Intracellular inclusions containing mutant alpha 1-antitrypsin Z are propagated in the absence of autophagic activity. J Biol Chem 281:4467–4476
92. Yam GHF, Gaplovska-Kysela K, Zuber C, Roth J (2007) Aggregated myocilin induces Russell bodies and causes apoptosis - Implications for the pathogenesis of myocilin-caused primary open-angle glaucoma. Am J Pathol 170:100–109
93. Schelhaas M, Malmstrom J, Pelkmans L, Haugstetter J, Ellgaard L, Grunewald K, Helenius A (2007) Simian Virus 40 depends on ER protein folding and quality control factors for entry into host cells. Cell 131:516–529
94. Lilley BN, Gilbert JM, Ploegh HL, Benjamin TL (2006) Murine polyomavirus requires the endoplasmic reticulum protein Derlin-2 to initiate infection. J Virol 80:8739–8744